Application of the finite difference heterogeneous multiscale method to the Richards' equation

Fulai Chen[1] and Li Ren[1]

Received 17 June 2007; revised 13 October 2007; accepted 2 January 2008; published 24 July 2008.

[1] This paper extends the finite difference heterogeneous multiscale method (FDHMM) to simulate transient unsaturated water flow problems in random porous media. The numerical method is based on the use of two different schemes for the original equation, at different grid levels which allows numerical results at a lower cost than solving the original equations. The main feature of FDHMM is that the necessary data for the macroscopic model are supplied by solving the microscopic model on a sparse spatial domain. The generated code is verified by applying the linearization model of the Richards' equation. Considering two different constitutive relationships, this method is applied to several test examples with different soil textures and boundary conditions. Both the Dirichlet and the periodic boundary conditions are considered for solving the local microscopic model when the water flow in heterogeneous unsaturated soils is simulated by FDHMM. The numerical experiments demonstrate that FDHMM can effectively simulate the transient unsaturated water flow in the specific soils. The numerical experiments also demonstrate that FDHMM can achieve accurate global mass balance and is a globally convergent algorithm, and the spatial correlation length of random coefficients under the specific standard deviation has relatively little influence on the accuracy of the method.

Citation: Chen, F., and L. Ren (2008), Application of the finite difference heterogeneous multiscale method to the Richards' equation, *Water Resour. Res.*, *44*, W07413, doi:10.1029/2007WR006275.

1. Introduction

[2] Modeling of nonequilibrium flow and transport in unsaturated soils/rocks has received increasing attention during recent years since it concerns such vital problems as protection of groundwater aquifers or securing of waste depositories [*Lewandowska et al.*, 2004]. Despite the increased ability to model subsurface heterogeneity provided by stochastic simulation methods [e.g., *Mantoglou and Wilson*, 1982; *Tompson et al.*, 1989; *Gutjahr et al.*, 1994; *Zhang et al.*, 1996], it is very difficult to simulate this kind of relative realistic situation by using classical finite difference method or finite element method based on smaller scale for our restricted computational capabilities. There is a corresponding increase in the need for new numerical techniques to accommodate heterogeneity of hydrodynamic parameters. The traditional approach for such problems is to obtain either analytically or empirically explicit equations for the scale of interest, eliminating other scales in the problem [*E and Engquist*, 2003]. Recently, several different but related multiscale approaches for problems with oscillating coefficients have been proposed, such as the multiscale finite element method (MSFEM) [*Hou and Wu*, 1997; *Hou et al.*, 1999], the heterogeneous multiscale method (HMM) [*E and Engquist*, 2003] and the numerical homogenization method [*Efendiev and Pankov*, 2004]. Here we should also mention the work of Babuška in the 70's which motivated the so-called multiscale finite element method [*Babuška*, 1976a, 1976b, 1977]. These multiscale methods not only target the full problem with the original resolution and attempt to capture the fine scale behavior of the solution directly on coarser grids, but also attempt to resolve scales below the coarse grid scale by doing a significant amount of local work [*He and Ren*, 2005]. Besides, in multiscale methods the coarse equations, which are required in upscaling procedures, are generally not expressed analytically, but rather formed and solved numerically, so that the fine scale information of the differential operator is carried throughout the simulation [*He and Ren*, 2006a].

[3] More recently, these multiscale methods have been developed and applied to the linear elliptic and parabolic equations which stem from the applications of the saturated flow in heterogeneous porous media [e.g., *Ye et al.*, 2004; *Abdulle and E*, 2003; *Aarnes et al.*, 2005; *He and Ren*, 2005, 2006b; *Durlofsky et al.*, 2007]. For applying and developing multiscale methods to nonlinear problems or unsaturated flow and transport problems in heterogeneous porous media, the published literature is limited. *Efendiev et al.* [2004] presented an extension of MSFEM to nonlinear problems by considering a multiscale map instead of the base functions that were considered in linear MSFEM, and applied the multiscale finite volume element method to Richards' equation describing water flow in unsaturated porous media. *He and Ren* [2006a] incorporated main ideas of both the Slodicka linear relaxation approximation scheme and MSFEM, and proposed a multiscale finite element linearization scheme to solve 2-D unsaturated water flow problems. The goal of this method is to obtain the large-

[1]Department of Soil and Water Sciences, China Agricultural University, and Key Laboratory of Plant-Soil Interactions, MOE, Beijing, China.

0043-1397/08/2007WR006275$09.00

scale solution of Richards' equation with heterogeneous coefficients accurately on a coarse grid without resolving all the small-scale details. *E et al.* [2005] used HMM to theoretically analyze linear and nonlinear elliptic homogenization problem, and estimated the error between the numerical solutions of HMM and the solutions of the homogenized equation. Moreover, *Yue and E* [2005] developed HMM for linear and nonlinear transport equations with multiscale velocity fields in heterogeneous porous media and focused on the problem in which advection is dominant at the small scale. *Efendiev and Pankov* [2004] proposed the numerical homogenization method to solve nonlinear random parabolic equations and applied the method to the 2-D convection-diffusion equation. This method uses general finite element procedure and solves local problems that are further coupled in the global formulation. Obviously, applications and developments of multiscale method to unsaturated flow and transport problems in heterogeneous porous media are currently being pursued. Numerical models of transient unsaturated flow in heterogeneous media are commonly based upon the solution of the well-known Richards' equation [e.g., *Farthing et al.*, 2003; *Miller et al.*, 2006]. From the previous introduction, so far MSFEM has had a successful application in the Richards' equation [*Efendiev et al.*, 2004; *He and Ren*, 2006a], but there's no work on applying HMM or numerical homogenization method to research this equation. Here, we plan to extend a multiscale method based on the framework of HMM to solve the Richards' equation with geostatistical random coefficients.

[4] Most of the multiscale methods presented to date have been limited to the finite element method. To the best of our knowledge, there is no literature on using multiscale techniques based on the finite difference method to deal with the unsaturated flow problems in heterogeneous porous media. In fact, there are also many widely used finite difference flow and solute transport models in both the groundwater and oil industries today, for example, MODFLOW, the modular finite difference groundwater flow model, is one of the most popular groundwater modeling programs [*Winston*, 1999]. Considering that the finite difference method plays an important role in numerical simulation, *Abdulle and E* [2003] proposed the finite difference heterogeneous multiscale method (FDHMM) based on the framework of HMM, and applied it to deal with linear parabolic homogenization problems. The method emphasizes theoretical analysis and considers the cell problem subject to the periodic boundary to deal with the multiscale parabolic equation with periodic and rough nonperiodic coefficients, it embodies well the computational simplicity and efficiency of finite differences. FDHMM includes a ''heterogeneous'' discretization which cares about the fine scale only on small representative region of the spatial domain, that is, FDHMM relies on the use of two different schemes for the original equation, at different grid levels which allows numerical results at a much lower cost than solving the original equations [*Abdulle and E*, 2003]. In this paper, we will demonstrate how the FDHMM can be used to simulate the unsaturated water flow problems in random porous media.

[5] *Yue and E* [2007] pointed out that crucial to both accuracy and efficiency of HMM are the boundary conditions that we impose on the microscale problems. These boundary conditions are in some sense artificial— they are required only because the computational domains are truncated and localized. *Durlofsky* [1991] noted that the use of periodic boundary conditions is common for a variety of problems involving effective media calculations and flow simulations even when the system is not strictly periodic. *Efendiev and Pankov* [2004] selected the local problem subject to the Dirichlet boundary to study the numerical homogenization of nonlinear random parabolic equations. Based on the careful choice of local problems, as well as the formulation of the discrete problem, they proved the convergence of the numerical method to the homogenized solution of the equation. If we apply the Dirichlet or periodic boundary condition to the local microscale problem in FDHMM, what level of accuracy could be obtained for extending this algorithm to simulate the transient unsaturated water flow problems (i.e., nonlinear parabolic problems) with random coefficients and the Dirichlet or Neumann infiltration boundary condition?

[6] An other feature of our numerical scheme is the formulae estimating the macroscopic flux in which the unsaturated hydraulic conductivity can be calculated as a diagonal tensor. In order to determine a unique and symmetric hydraulic conductivity tensor, similar to the assumption defined by *Yeh et al.* [1985], and *Mantoglou and Gelhar* [1987], here we also assume ''unsaturated hydraulic conductivity tensor'' with principal axes oriented in the direction of the principal statistical anisotropy axes of the local parameters, which means that the unsaturated hydraulic conductivity tensor is diagonal.

[7] Taking a backward Euler method to Richards' equation in time, one obtains a set of nonlinear parabolic equations arising from a fully implicit finite difference discretization at per time-step in the cell problem. For quickly solving the resulting linear equations in iteration, we choose the multigrid method to solve large sparse systems of linear equations as a part of our algorithm. This multigrid algorithm is incorporated in the numerical simulator MGD9V [*de Zeeuw*, 1990]. For the principle of choosing cell size, *Abdulle and E* [2003] and *E et al.* [2005] proposed that cell size should be larger than the correlation length of the random coefficients to deal with the linear problems. However, HMM proceeds as a standard finite element method with the usual basis functions. The new component comes in the computation of the stiffness matrix which is obtained by solving a small ''cell problem'' on each element. This flexibility of HMM means that it may be applied to the problem for which the microstructure can't be entirely found beforehand [see *E and Engquist*, 2003]. Although using the finite difference scheme, FDHMM inherits this advantage of HMM and may also deal with the problem for which the microstructure has been partly found beforehand. For this problem it is sometimes difficult to obtain an explicit correlation length of the random coefficients, it may be easy to choose the cell size as per the coarse mesh size. Here we try to find a more applicable principle of choosing cell size.

[8] The rest of this paper begins with a brief introduction of the transient unsaturated flow equation in porous media and the constitutive relationship used to close the equation. Next an elaborate explanation of the numerical method used

herein is described. Numerical results are presented to illustrate the discussed algorithm under the cases of different soils with two infiltration boundary conditions (the Dirichlet infiltration boundary condition and the Neumann infiltration boundary condition) and two constitutive relationships (the van Genuchten-Mualem model and the Gardner-Basha model). This is followed by a general discussion of the method, via a transient unsaturated water flow problem with the van Genuchten-Mualem model and the Dirichlet infiltration boundary. The application scope and limitations of our method are also pointed out. Last, some conclusions are given.

2. Introduction to FDHMM

2.1. Governing Equation and Constitutive Relationships

[9] Let ψ and θ denote the pressure head and the volumetric water content respectively. Three standard forms of the Richards' equation may be identified: the ψ-based form, the θ-based form, and the mixed form [*Celia et al.*, 1990]. A solution using the ψ-based formulation and a backward Eular time discretization is shown to produce unacceptably large mass balance errors for many example calculations [e.g., *van Genuchten*, 1982; *Allen and Murphy*, 1985; *Celia et al.*, 1990]. A numerical scheme which solves a mixed form has been proposed to overcome mass conservation difficulties, while maintaining the advantages of the ψ-based formulation [*Allen and Murphy*, 1985; *Celia et al.*, 1990; *Rathfelder and Abriola*, 1994; *Efendiev et al.*, 2004; *He and Ren*, 2006a]. Thus the mixed form Richards' equation is used as our model for transient unsaturated flow with the absence of sources and sinks in porous media. The governing equation is

$$\frac{\partial\theta(\psi)}{\partial t} - \nabla\cdot[\mathbf{K}(\mathbf{x},\psi)\nabla(\psi - z)] = 0, \tag{1}$$

where $\mathbf{K}(\mathbf{x}, \psi)$ is the unsaturated hydraulic conductivity, $\mathbf{x} = (x, z)$ is the spatial coordinate, and z denotes the vertical coordinate that is positively oriented downward and t is time.

[10] The constitutive relationship to describe hydraulic properties must be selected prior to application of the numerical solution of the unsaturated flow model. For our comparisons, we are interested mainly in two soil hydraulic conductivity functions in widespread used: the van Genuchten-Mualem model and the Gardner-Basha model.

[11] The van Genuchten-Mualem model [*van Genuchten*, 1980] has it that the van Genuchten soil-water retention associates hydraulic conductivity functions with the Mualem substitution [*Mualem*, 1976], and is defined as follows

$$\begin{aligned}
&\theta(\psi) = \theta_r + (\theta_s - \theta_r)\left[1 + (\alpha_v|\psi|)^{n\prime}\right]^{-m\prime},\\
&K(\mathbf{x},\psi) = K_s(\mathbf{x})K_r(\psi) = K_s(\mathbf{x})\frac{\left\{1-(\alpha_v|\psi|)^{n'-1}\left[1+(\alpha_v|\psi|)^{n'}\right]^{-m'}\right\}^2}{\left[1+(\alpha_v|\psi|)^{n'}\right]^{\frac{m'}{2}}}\\
&m' = 1 - \tfrac{1}{n'},
\end{aligned} \tag{2}$$

where θ_r is the residual water content, θ_s is the saturated water content, n' and m' are empirical parameters relating to the pore size distribution, K_s is the saturated hydraulic conductivity, and α_v is the parameter related to the mean pore size. $C(\psi) \equiv d\theta/d\psi$ is the specific moisture capacity function and has the following formulation in this van Genuchten-Mualem model,

$$C(\psi) = (\theta(\psi) - \theta_r)\frac{(n'-1)\alpha_v(\alpha_v|\psi|)^{n'-1}}{1 + (\alpha_v|\psi|)^{n'}}. \tag{3}$$

[12] Combining the Gardner equation [*Gardner*, 1958], *Basha* [1999] used an exponential model, the Gardner-Basha model, to describe soil properties. The Gardner-Basha model has the following constitutive relation formulations

$$\begin{aligned}
&\theta(\psi) = \theta_r + (\theta_s - \theta_r)e^{-\beta|\psi|},\\
&K(\mathbf{x},\psi) = K_s(\mathbf{x})K_r(\psi) = K_s(\mathbf{x})e^{-\alpha_G|\psi|},
\end{aligned} \tag{4}$$

where α_G, β are parameters of the porous media. θ_r will be assumed to be zero in the following. According to the Gardner-Basha model, one obtains

$$C(\psi) = \beta(\theta_s - \theta_r)e^{-\beta|\psi|}. \tag{5}$$

2.2. Principle and Algorithm of FDHMM

[13] FDHMM presented by *Abdulle and E* [2003] inherits the advantages of HMM. HMM is a general methodology that allows us to efficiently move between the macroscopic and microscopic models, and to best exploit scale separation in the problem for improving efficiency [*E and Engquist*, 2003]. The key to efficiency of such an approach is the possibility that the microscopic model does not have to be solved over the whole computational domain, but rather over a small region near where data estimation is carried out [*E et al.*, 2003]. *Abdulle and E* [2003] embodied the idea of HMM to the finite difference scheme, presented finite difference HMM (FDHMM) and applied it to the multiscale linear parabolic equation. Here, we extend FDHMM to nonlinear parabolic problems for simulating unsaturated water flows in heterogeneous soils with random hydraulic parameters.

[14] Put briefly, the overall scheme for FDHMM contains two main components. The first is a macroscopic scheme, in which a macroscopic equation is evolved on a coarse mesh (the mesh of interest) with unknown data recovered from the solution of the microscopic model. This macroscopic scheme does not rely on whether or not the macroscopic model is explicitly known. The second component is a microscopic scheme, in which the original equation is solved on a sparse (heterogeneous) spatial domain. There are divided into four steps for implementing this scheme.

[15] (1) Reconstruction for cell problem. To start the evolution with the cell problem, the initial values and boundary conditions of the cell problem are reconstructed according to the coarse solution Ψ^n at the former time-step t^n.

[16] (2) Microscopic evolution. A set of original equations with given initial values and boundary conditions are solved in every cell. In these cells, the fine solution ψ^{n+1} at

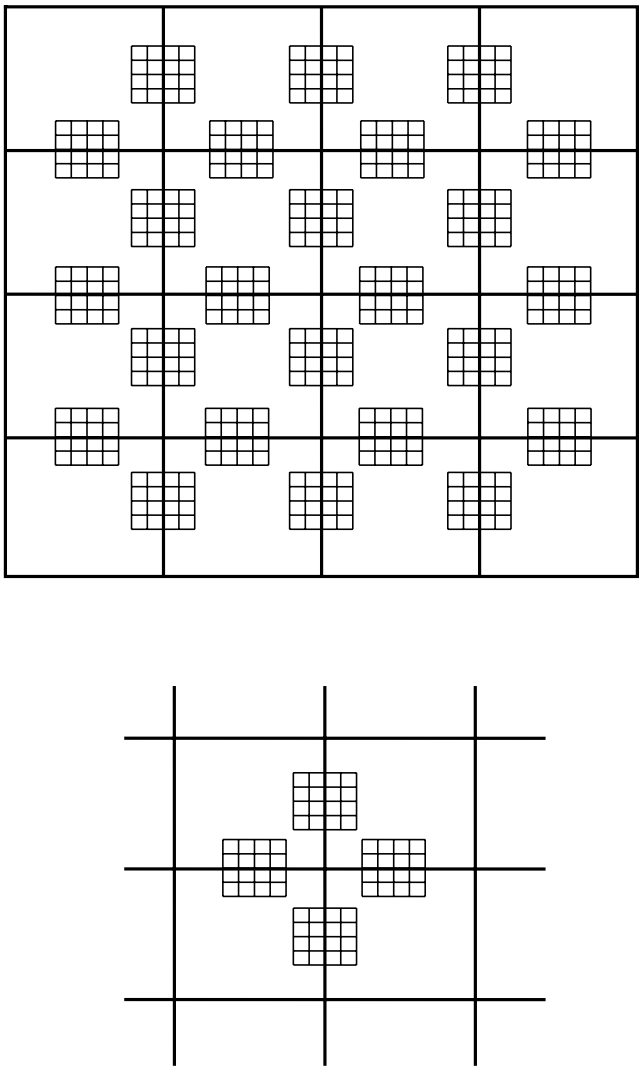

Figure 1. Schematic showing fine- and coarse-scale meshes (top) and δ-cell at the coarse node (bottom).

the next time-step t^{n+1} are obtained, that is, the fine scale information at t^{n+1} is obtained.

[17] (3) Estimating macroscopic flux. The macroscopic flux F at the time t^{n+1} is estimated as an average of the microscopic fluxes.

[18] (4) Macroscopic evolution. The macroscopic equation

$$\frac{\partial \Theta(\Psi)}{\partial t} = -\nabla \cdot F, \tag{6}$$

is solved at the coarse mesh, where Θ is the macroscopic volumetric water content, Ψ is the macroscopic pressure head corresponding to ψ, F is the macroscopic flux tensor. Then the coarse solution Ψ^{n+1} at the next time-step t^{n+1} is obtained. We may notice that the macroscopic equation (6) is not an explicit expression and this equation can express the macroscopic behavior in that it is obtained according to the principle of the flux balance.

[19] We now discuss this algorithm in more detail. For simplicity, we assume that the solution domain Ω is a square and a coarse equidistant mesh is constructed by uniformly dividing Ω into $N \times N$ subrectangles. (x_i, y_j) is the coordinate of the corresponding node (i,j), $i,j = 1,\cdots,N+1$. $H = x_{i+1}\text{-}x_i = y_{j+1}\text{-}y_j$ denotes the mesh size.

2.2.1. Step 1: Reconstruction for Cell Problem

[20] We first determine the position of the control volume, i.e., the cell, at the coarse mesh. We center the cell at the midpoint of the line segment connecting any two neighboring nodes except of two exterior nodes, and let it be a square cell of size δ. Thus there are four δ-cells $I^{\delta}_{i\pm\frac{1}{2},j}$, $I^{\delta}_{i,j\pm\frac{1}{2}}$ around every interior coarse node (i,j) (Figure 1). Set $d_- = \frac{(H-\delta)}{2}$, $d_+ = \frac{(H+\delta)}{2}$, then $I^{\delta}_{i\pm\frac{1}{2},j}$, $I^{\delta}_{i,j\pm\frac{1}{2}}$ are defined as follows

$$\begin{aligned} I^{\delta}_{i\pm\frac{1}{2},j} &= [x_i \pm d_-, x_i \pm d_+] \times \left[y_j - \tfrac{\delta}{2}, y_j + \tfrac{\delta}{2}\right],\ i,j = 2,\cdots,N, \\ I^{\delta}_{i,j\pm\frac{1}{2}} &= \left[x_i - \tfrac{\delta}{2}, x_i + \tfrac{\delta}{2}\right] \times [y_j \pm d_-, y_j \pm d_+],\ i,j = 2,\cdots,N. \end{aligned} \tag{7}$$

In the following we will denote any cell by I^{δ}. Next, I^{δ} is uniformly divided into a fine $M \times M$ mesh and the node in it

is denoted by (k, l), $k, l = 1, \cdots, M+1$. The coordinates (ξ_k, η_l) are yielded by

$$\begin{aligned} \xi_k &= \frac{H-\delta}{2} + (k-1)\frac{\delta}{M}, \quad k = 1, \cdots, M+1, \\ \eta_l &= \frac{H-\delta}{2} + (l-1)\frac{\delta}{M}, \quad l = 1, \cdots, M+1. \end{aligned} \tag{8}$$

[21] Suppose $\Psi^n_{i,j}$, a coarse numerical solution of equation (6) on the coarse node (i,j) at time t^n. In every cell, initial values and boundary conditions for the cell problem can be determined by a reconstruction from $\Psi^n_{i,j}$.

[22] We first define a reconstruction from $\Psi^n_{i,j}$ by the piecewise linear reconstruction.

$$\begin{aligned} \psi^n_{k,l} &= \Psi^n_{i-1,j} + \xi_k \frac{\Psi^n_{i,j} - \Psi^n_{i-1,j}}{H}, \quad \text{for} \quad I^\delta_{i-\frac{1}{2},j}, \\ \psi^n_{k,l} &= \Psi^n_{i,j} + \xi_k \frac{\Psi^n_{i+1,j} - \Psi^n_{i,j}}{H}, \quad \text{for} \quad I^\delta_{i+\frac{1}{2},j}, \\ \psi^n_{k,l} &= \Psi^n_{i,j-1} + \eta_l \frac{\Psi^n_{i,j} - \Psi^n_{i,j-1}}{H}, \quad \text{for} \quad I^\delta_{i,j-\frac{1}{2}}, \\ \psi^n_{k,l} &= \Psi^n_{i,j} + \eta_l \frac{\Psi^n_{i,j+1} - \Psi^n_{i,j}}{H}, \quad \text{for} \quad I^\delta_{i,j+\frac{1}{2}}, \end{aligned} \tag{9}$$

where $\psi^n_{k,l}$ is the reconstruction value of fine node (k,l) at time t^n, $k,l = 1,\cdots,M+1$. It means that $\psi^n_{k,l}$ is reconstructed along the x-direction for the cells $I^\delta_{i\pm\frac{1}{2},j}$ and along the z-direction for the cells $I^\delta_{i,j\pm\frac{1}{2}}$ respectively.

[23] For the cell problem in the time interval $[t^n, t^{n+1}]$, initial values $\psi(\mathbf{x}, t^n)$ can be defined as follows

$$\psi(\mathbf{x}, t^n) = \psi^n(\mathbf{x}) \quad \text{in} \quad I^\delta. \tag{10}$$

[24] A key ingredient in FDHMM is the formulation, particularly the boundary conditions, of the microscale model. We will discuss the two boundary conditions: the periodic boundary condition, and the Dirichlet boundary condition. These have been used in one way or another in previous literature [see *Durlofsky*, 1991; *Abdulle and E*, 2003; *Efendiev and Pankov*, 2004; *E et al.*, 2005]. For the periodic boundary condition, the local microscale problem is subject to the following boundary condition:

$$\psi(\mathbf{x}, t) - \psi^n(\mathbf{x}) \text{ is periodic with period } I^\delta. \tag{11}$$

this can be described clearly as follows

$$\begin{aligned} \psi_{k,0} &= \psi_{k,M} + \psi^n_{k,0} - \psi^n_{k,M}, \quad k = 1, \cdots, M+1, \\ \psi_{M+2,l} &= \psi_{2,l} + \psi^n_{M+2,l} - \psi^n_{2,l}, \quad l = 1, \cdots, M+1, \end{aligned} \tag{12}$$

with similar formulas for $\psi_{0,l}$ and $\psi_{k,M+2}$ [see *Abdulle and E*, 2003]. To more close the discrete model, we may also use the following discrete form of (11):

$$\begin{aligned} \psi_{k,0} &= \psi_{k,M} + \psi^n_{k,0} - \psi^n_{k,M}, \quad k = 1, \cdots, M+1, \\ \psi_{k,1} &= \psi_{k,M+1} + \psi^n_{k,1} - \psi^n_{k,M+1}, \quad k = 1, \cdots, M+1, \\ \psi_{M+1,l} &= \psi_{1,l} + \psi^n_{M+1,l} - \psi^n_{1,l}, \quad l = 1, \cdots, M+1, \\ \psi_{M+2,l} &= \psi_{2,l} + \psi^n_{M+2,l} - \psi^n_{2,l}, \quad l = 1, \ldots, M+1, \end{aligned} \tag{13}$$

with similar formulas for $\psi_{0,l}$, $\psi_{1,l}$, $\psi_{k,M+1}$ and $\psi_{k,M+2}$. The Dirichlet boundary condition is such that

$$\psi(\mathbf{x}, t) = \psi^n(\mathbf{x}), \quad \text{on} \quad \partial I^\delta, \tag{14}$$

it can be expressed more clearly as

$$\begin{aligned} \psi_{k,1} = \psi^n_{k,1}, \psi_{k,M+1} = \psi^n_{k,M+1}, \; k = 1, \cdots, M+1, \\ \psi_{1,l} = \psi^n_{1,l}, \psi_{M+1,l} = \psi^n_{M+1,l}, \; l = 1, \cdots, M+1. \end{aligned} \tag{15}$$

2.2.2. Step 2: Microscopic Evolution

[25] After defining the initial values and the boundary conditions, in each cell I^δ, we need to solve the original equation (1) subject to (10) and (11), or the original equation (1) subject to (10) and (14).

[26] A problem is how to choose macro- and micro-time steps. *Abdulle and E* [2003] solved the cell problems with a micro-time step in a time interval much shorter than the macro-time step to deal with the linear problem. However, considering the complexity resulting from the nonlinearity of unsaturated flow problems, a large macro-time steps may make our algorithm inefficient. To assure the efficiency of the algorithm used, we take a small macro-time step and let the micro-time step be equal to the macro-time one. If temporal discretization of (1) uses a backward Euler method, the standard fully implicit finite difference approximation of (1) may be written as

$$\begin{aligned} \frac{\theta^{n+1,m+1}_{k,l} - \theta^n_{k,l}}{\Delta t} &- \frac{1}{\Delta\xi}\left[K^{n+1,m}_{k+\frac{1}{2},l}\frac{\psi^{n+1,m+1}_{k+1,l} - \psi^{n+1,m+1}_{k,l}}{\Delta\xi}\right. \\ &\left. - K^{n+1,m}_{k-\frac{1}{2},l}\frac{\psi^{n+1,m+1}_{k,l} - \psi^{n+1,m+1}_{k-1,l}}{\Delta\xi}\right] \\ &- \frac{1}{\Delta\eta}\left[K^{n+1,m}_{k,l+\frac{1}{2}}\frac{\psi^{n+1,m+1}_{k,l+1} - \psi^{n+1,m+1}_{k,l}}{\Delta\eta}\right. \\ &\left. - K^{n+1,m}_{k,l-\frac{1}{2}}\frac{\psi^{n+1,m+1}_{k,l} - \psi^{n+1,m+1}_{k,l-1}}{\Delta\eta}\right] \\ &+ \frac{1}{\Delta\eta}\left(K^{n+1,m}_{k,l+\frac{1}{2}} - K^{n+1,m}_{k,l-\frac{1}{2}}\right) = 0, \end{aligned} \tag{16}$$

where $\Delta t = t^{n+1} - t^n$ is the time step size, $\Delta\xi, \Delta\eta$ are the fine mesh spacing for x- and z-direction, n and m are the time and iteration levels respectively, $\psi^{n+1,0}_{k,l} = \psi^n_{k,l}$, $K_{k+\frac{1}{2},l} = (K_{k+1,l}K_{k,l})^{\frac{1}{2}}$ denotes the geometric mean between $K_{k+1,l}$ and $K_{k,l}$, similarly for $K_{k-\frac{1}{2},l}$ and $K_{k,l\pm\frac{1}{2}}$. In fact, the geometric mean for $K_{k\pm\frac{1}{2},l}$ and $K_{k,l\pm\frac{1}{2}}$ is usually preferable over the arithmetic mean [*Haverkamp and Vauclin*, 1979; *Hornung and Messing*, 1983].

[27] The key to (16) is the expansion of $\theta^{n+1,m+1}_{k,l}$ in a truncated Taylor series with respect to ψ, about the expansion point $\psi^{n+1,m}_{k,l}$. If all terms higher than linear are neglected, there results [*Celia et al.*, 1990]

$$\theta^{n+1,m+1}_{k,l} \approx \theta^{n+1,m}_{k,l} + C^{n+1,m}_{k,l}\left(\psi^{n+1,m+1}_{k,l} - \psi^{n+1,m}_{k,l}\right). \tag{17}$$

[28] Substituting (17) into (16), let $\Delta\xi = \Delta\eta = a$, and putting all the unknowns on the left-hand and all the knows on the right-hand side, we have

$$\begin{aligned}
&-\frac{1}{a^2}K^{n+1,m}_{k,l-\frac{1}{2}}\psi^{n+1,m+1}_{k,l-1} - \frac{1}{a^2}K^{n+1,m}_{k-\frac{1}{2},l}\psi^{n+1,m+1}_{k-1,l}\\
&+\left[\frac{1}{\Delta t}C^{n+1,m}_{k,l} + \frac{1}{a^2}\left(K^{n+1,m}_{k,l-\frac{1}{2}} + K^{n+1,m}_{k,l+\frac{1}{2}} + K^{n+1,m}_{k-\frac{1}{2},l} + K^{n+1,m}_{k+\frac{1}{2},l}\right)\right]\psi^{n+1,m+1}_{k,l}\\
&-\frac{1}{a^2}K^{n+1,m}_{k+\frac{1}{2},l}\psi^{n+1,m+1}_{k+1,l} - \frac{1}{a^2}K^{n+1,m}_{k,l+\frac{1}{2}}\psi^{n+1,m+1}_{k,l+1}\\
&= -\frac{1}{a}\left(K^{n+1,m}_{k,l+\frac{1}{2}} - K^{n+1,m}_{k,l-\frac{1}{2}}\right) - \frac{1}{\Delta t}\left(\theta^{n+1,m}_{k,l} - \theta^{n}_{k,l}\right)\\
&+\frac{1}{\Delta t}C^{n+1,m}_{k,l}\psi^{n+1,m}_{k,l}. \qquad (18)
\end{aligned}$$

[29] Let

$$\begin{aligned}
\tilde{K}^{n+1,m}_{k,l} &= K^{n+1,m}_{k,l-\frac{1}{2}} + K^{n+1,m}_{k,l+\frac{1}{2}} + K^{n+1,m}_{k-\frac{1}{2},l} + K^{n+1,m}_{k+\frac{1}{2},l},\\
R^{n+1,m}_{k,l} &= -\frac{1}{a}\left(K^{n+1,m}_{k,l+\frac{1}{2}} - K^{n+1,m}_{k,l-\frac{1}{2}}\right) - \frac{1}{\Delta t}\left(\theta^{n+1,m}_{k,l} - \theta^{n}_{k,l}\right)\\
&\quad + \frac{1}{\Delta t}C^{n+1,m}_{k,l}\psi^{n+1,m}_{k,l}, \qquad (19)
\end{aligned}$$

then equation (18) can be simplified as follows

$$\begin{aligned}
&-\frac{1}{a^2}K^{n+1,m}_{k,l-\frac{1}{2}}\psi^{n+1,m+1}_{k,l-1} - \frac{1}{a^2}K^{n+1,m}_{k-\frac{1}{2},l}\psi^{n+1,m+1}_{k-1,l}\\
&+\left(\frac{1}{\Delta t}C^{n+1,m}_{k,l} + \frac{1}{a^2}\tilde{K}^{n+1,m}_{k,l}\right)\psi^{n+1,m+1}_{k,l} - \frac{1}{a^2}K^{n+1,m}_{k+\frac{1}{2},l}\psi^{n+1,m+1}_{k+1,l}\\
&-\frac{1}{a^2}K^{n+1,m}_{k,l+\frac{1}{2}}\psi^{n+1,m+1}_{k,l+1} = R^{n+1,m}_{k,l}. \qquad (20)
\end{aligned}$$

[30] To solve the nonsymmetric nonlinear equation (20) using iteration, we consider to use the multigrid method which is among the fastest methods to solve large sparse systems of linear equations arising from the discretization of partial differential equations. For implementing this multigrid algorithm, we directly use a code MGD9V [*de Zeeuw*, 1990]. MGD9V is used to solve linear systems resulting from the 9-point discretization of a general linear second-order elliptic partial differential equation in two dimensions, this code is designed to solve problems which include dominant convection, discontinuous diffusion coefficients and highly stretched grid cells. The solver is based on multigrid with operator-dependent prolongations (and restrictions), automatic derivation of coarse grid matrices and incomplete line LU decomposition as a smoother.

[31] Setting error tolerance ε equal to 10^{-6} in our algorithm, the iteration stops if

$$|\psi^{n+1,m+1}_{k,l} - \psi^{n+1,m}_{k,l}| \le \varepsilon. \qquad (21)$$

2.2.3. Step 3: Estimation for Macroscopic Flux

[32] Based on the reasons described in section 1, we apply the assumption defined by *Yeh et al.* [1985] and *Mantoglou and Gelhar* [1987] to derive the macroscopic flux F,

$$\begin{aligned}
F &= -\frac{1}{|I^\delta|}\int\int_{I^\delta}\mathbf{K}(\mathbf{x},\psi)\nabla\left(\psi(\mathbf{x},t^{n+1}) - z\right)d\mathbf{x}\\
&= -\frac{1}{|I^\delta|}\int\int_{I^\delta}\begin{pmatrix} K_{xx} & 0\\ 0 & K_{zz}\end{pmatrix}\begin{pmatrix}\frac{\partial\psi}{\partial x}\\ \frac{\partial\psi}{\partial z} - 1\end{pmatrix}dxdz\\
&= -\frac{1}{|I^\delta|}\int\int_{I^\delta}\begin{pmatrix} K_{xx}\frac{\partial\psi}{\partial x}\\ K_{zz}\left(\frac{\partial\psi}{\partial z} - 1\right)\end{pmatrix}dxdz\\
&= \begin{pmatrix} F^x\\ F^z\end{pmatrix}, \qquad (22)
\end{aligned}$$

where F^x denotes the macroscopic flux estimated along the x-direction, F^z denotes the macroscopic flux estimated along the z-direction. Here we assume that at the fine scale, the porous medium exhibits no change in the unsaturated hydraulic conductivity with respect to direction, i.e., $K_{xx} = K_{zz}$.

[33] To estimate the macroscopic flux, *Abdulle and E* [2003] presented a feasible idea, which is to compute an average flux over a δ-cell. *E et al.* [2005] pointed out that a smaller cell $I^{\delta'}$ with $\delta' < \delta$ may be chosen to compute the average flux in order to reduce the effect of the imposed boundary condition on the cell problem. Here we follow these ideas to compute approximations of F^x and F^z as follows

$$\begin{aligned}
F^x &= -\frac{1}{|I^\delta|}\int\int_{I^\delta}K_{xx}\frac{\partial\psi}{\partial x}dxdz\\
&\approx -\frac{a^2}{\delta'^2}\sum_{k=2}^{M-1}\sum_{l=2}^{M-1}K^{n+1,m+1}_{k+\frac{1}{2},l}\frac{\psi^{n+1,m+1}_{k+1,l} - \psi^{n+1,m+1}_{k,l}}{a}, \quad \text{for } I^\delta_{i\pm\frac{1}{2},j},\\
F^z &= -\frac{1}{|I^\delta|}\int\int_{I^\delta}K_{zz}\left(\frac{\partial\psi}{\partial z} - 1\right)dxdz\\
&\approx -\frac{a^2}{\delta'^2}\sum_{k=2}^{M-1}\sum_{l=2}^{M-1}K^{n+1,m+1}_{k,l+\frac{1}{2}}\left(\frac{\psi^{n+1,m+1}_{k,l+1} - \psi^{n+1,m+1}_{k,l}}{a} - 1\right),\\
&\quad \text{for } I^\delta_{i,j\pm\frac{1}{2}}. \qquad (23)
\end{aligned}$$

2.2.4. Step 4: Macroscopic Evolution

[34] After knowing the macroscopic fluxes, we may evolve the macroscopic equation (6) on the coarse mesh with a time step size Δt. Macroscopic evolution is done via the approximation of (6)

$$\frac{\Theta^{n+1}_{i,j} - \Theta^{n}_{i,j}}{\Delta t} = -\frac{F^x_{i+\frac{1}{2},j} - F^x_{i-\frac{1}{2},j} + F^z_{i,j+\frac{1}{2}} - F^z_{i,j-\frac{1}{2}}}{H}, \qquad (24)$$

then

$$\Theta^{n+1}_{i,j} = \Theta^{n}_{i,j} - \frac{\Delta t}{H}\left(F^x_{i+\frac{1}{2},j} - F^x_{i-\frac{1}{2},j} + F^z_{i,j+\frac{1}{2}} - F^z_{i,j-\frac{1}{2}}\right). \qquad (25)$$

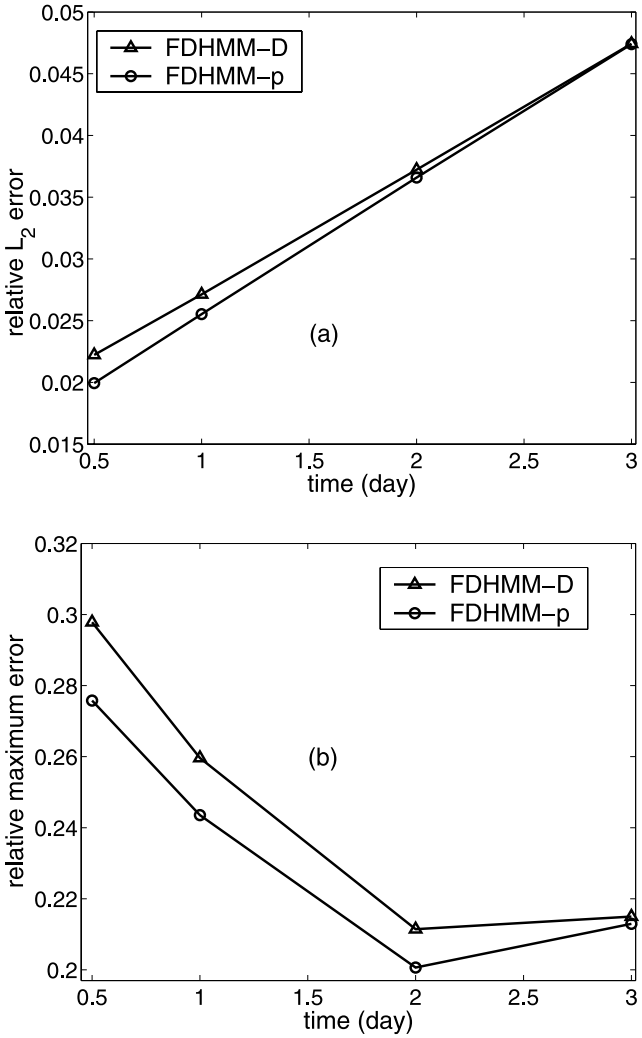

Figure 2. Relative (a) L_2 and (b) maximum errors between "exact" and two coarse solutions for the linearization model of Richards' equation with periodic coefficients.

According to the water retention function at point scale, the macroscopic pressure head $\Psi_{i,j}^{n+1}$ at coarse mesh point (i,j) may be estimated using the latest estimation of $\Theta_{i,j}^{n+1}$ at coarse mesh point (i,j). For the van Genuchten-Mualem model we have

$$\Psi_{i,j}^{n+1} = -\frac{1}{\alpha_{vi,j}}\left[\left(\frac{\theta_s - \theta_r}{\Theta_{i,j}^{n+1} - \theta_r}\right)^{1/m\prime} - 1\right]^{1/n\prime}. \tag{26}$$

For the Gardner-Basha model we have

$$\Psi_{i,j}^{n+1} = -\frac{1}{\beta}\ln\left(\frac{\theta_s - \theta_r}{\Theta_{i,j}^{n+1} - \theta_r}\right). \tag{27}$$

[35] Thus the algorithm of FDHMM is completed.

3. Numerical Experiments

[36] In this section, a series of numerical experiments are used to demonstrate the capabilities of the discussed algorithm, we will solve the microscale problem with two different boundary conditions: the Dirichlet and periodic boundary conditions. For convenience, we set that FDHMM-D stands for FDHMM with the Dirichlet boundary condition for local microscale problem, and FDHMM-p stands for FDHMM with the periodic boundary condition for local microscale problem. The coarse-grid models are compared with the fine-scale models solved on a fine mesh. Because Richards' equation is nonlinear, analytical solution is impossible except for special cases. Therefore the reference solution has been computed by the classical finite difference method with multigrid on a fine mesh, we will often refer to this solution as the "exact" solution.

[37] As a measure for the error we take the relative L_2 norm and the relative maximum norm

$$eer_2 = \left[\frac{\sum_{i=1}^{N'}\left(\Psi_i - \Psi(\mathbf{x}_i)\right)^2}{\sum_{i=1}^{N'}\left(\Psi(\mathbf{x}_i)\right)^2}\right]^{\frac{1}{2}},$$
$$eer_\infty = \frac{\max_{i=1,\cdots,N'}|\Psi_i - \Psi(\mathbf{x}_i)|}{\max_{i=1,\cdots,N'}|\Psi(\mathbf{x}_i)|}, \tag{28}$$

respectively, where N' is the total number of nodes on the coarse mesh, Ψ_i denotes the coarse solution at $\mathbf{x}_i$, $\Psi(\mathbf{x}_i)$ denotes the reference solution projected on the coarse mesh, i.e., $\Psi(\mathbf{x}_i)$ is the "exact" solution of ψ at the corresponding node.

[38] In this paper, the heterogeneity in porous media comes from the saturated hydraulic conductivity K_s and the model parameter α. Field studies indicate that the saturated hydraulic conductivity field in heterogeneous media follows a lognormal distribution [e.g., *Freeze*, 1975; *Gelhar*, 1986; *Tompson and Gelhar*, 1990; *Neuman and Orr*, 1993; *Koltermann and Gorelick*, 1996]. Similarly, it has been observed that the distribution of the model parameter α is lognormal [*Russo and Bouton*, 1992]. So we assume that K_s and α follow a lognormal distribution and their spatially correlated random fields are generated with a random field generator TBM [*Mantoglou and Wilson*, 1982] which is a technique to create artificial fields of physical quantities perceived to be random in various statistical or stochastic models of natural processes [*Tompson et al.*, 1989].

[39] In all test examples, the study domain Ω is a rectangle covering 10.0 m × 10.0 m with point (0,0) as the origin of coordinate. A uniform finite difference mesh is constructed by uniformly dividing Ω into a $N \times N$ mesh. The coarse mesh is 32 × 32 and the coarse solutions are obtained by using the multiscale methods on this mesh. The fine mesh is 256 × 256, the "exact" solution and random fields of K_s and α are obtained on this mesh. Cell size δ should be chosen such that $K(\mathbf{x}, \psi)$ restricted to I^δ gives an accurate enough representation of the local variations of $K(\mathbf{x}, \psi)$. In this section, for simplicity, we choose δ equal to H which means that the microscopic information of the study domain is obtained entirely beforehand. Each cell is uniformly divided into an 8 × 8 mesh such that its mesh size is equal to the size of the fine mesh.

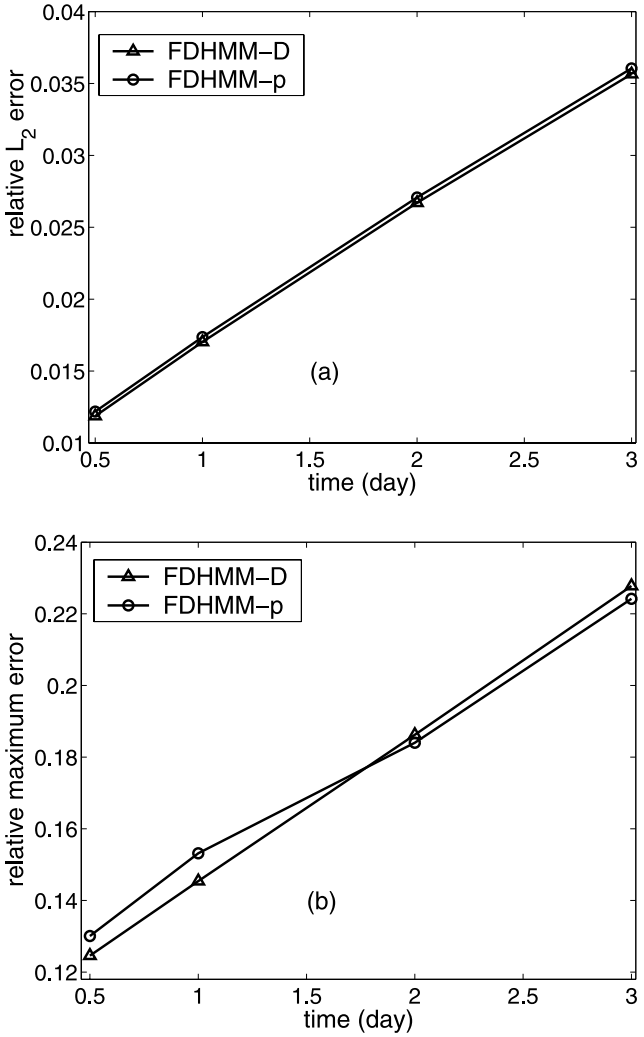

Figure 3. Relative (a) L_2 and (b) maximum errors between "exact" and two coarse solutions for the linearization model of Richards' equation with random coefficients.

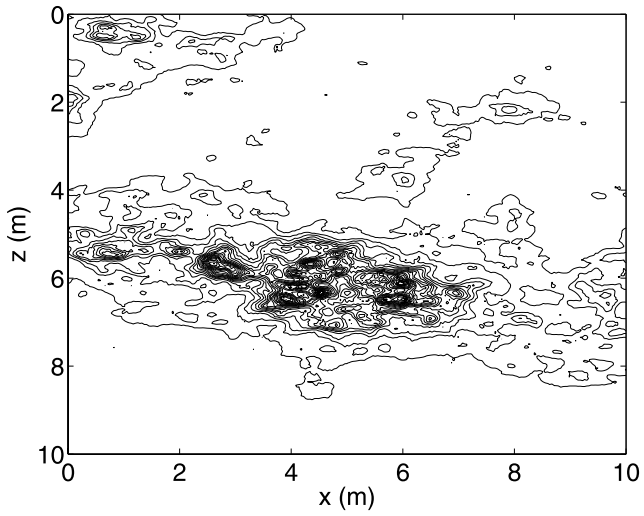

Figure 4. A realization of the random lognormal saturated conductivity field. The ratio of maximum to minimum is 7.4×10^2.

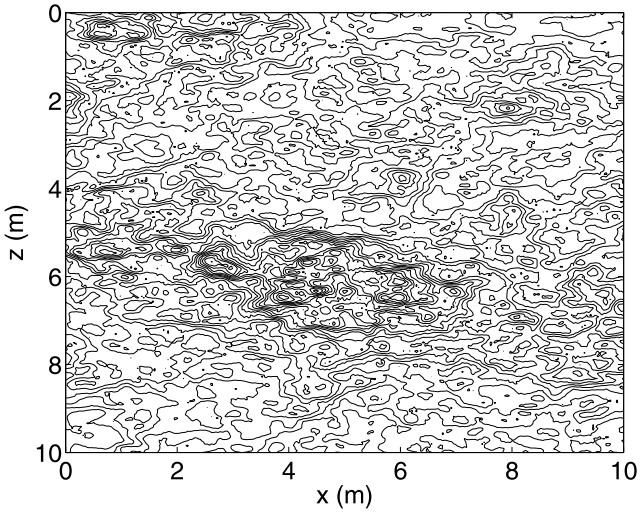

Figure 5. A realization of the random lognormal alpha field. The ratio of maximum to minimum is 5.2.

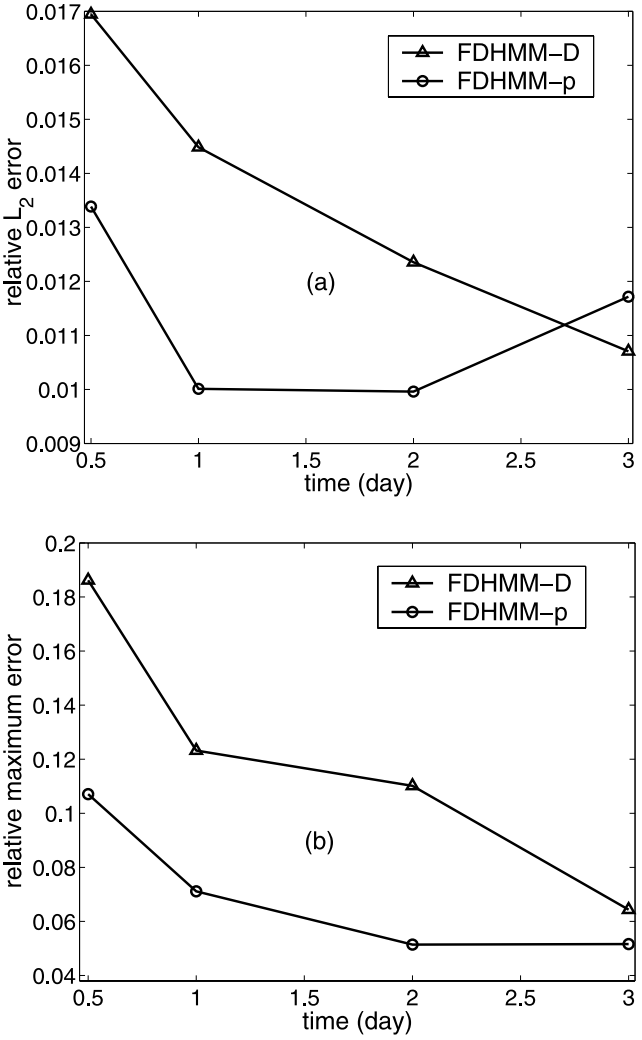

Figure 6. Relative (a) L_2 and (b) maximum errors between "exact" and two coarse solutions for van Genuchten-Mualem model with Dirichlet infiltration boundary.

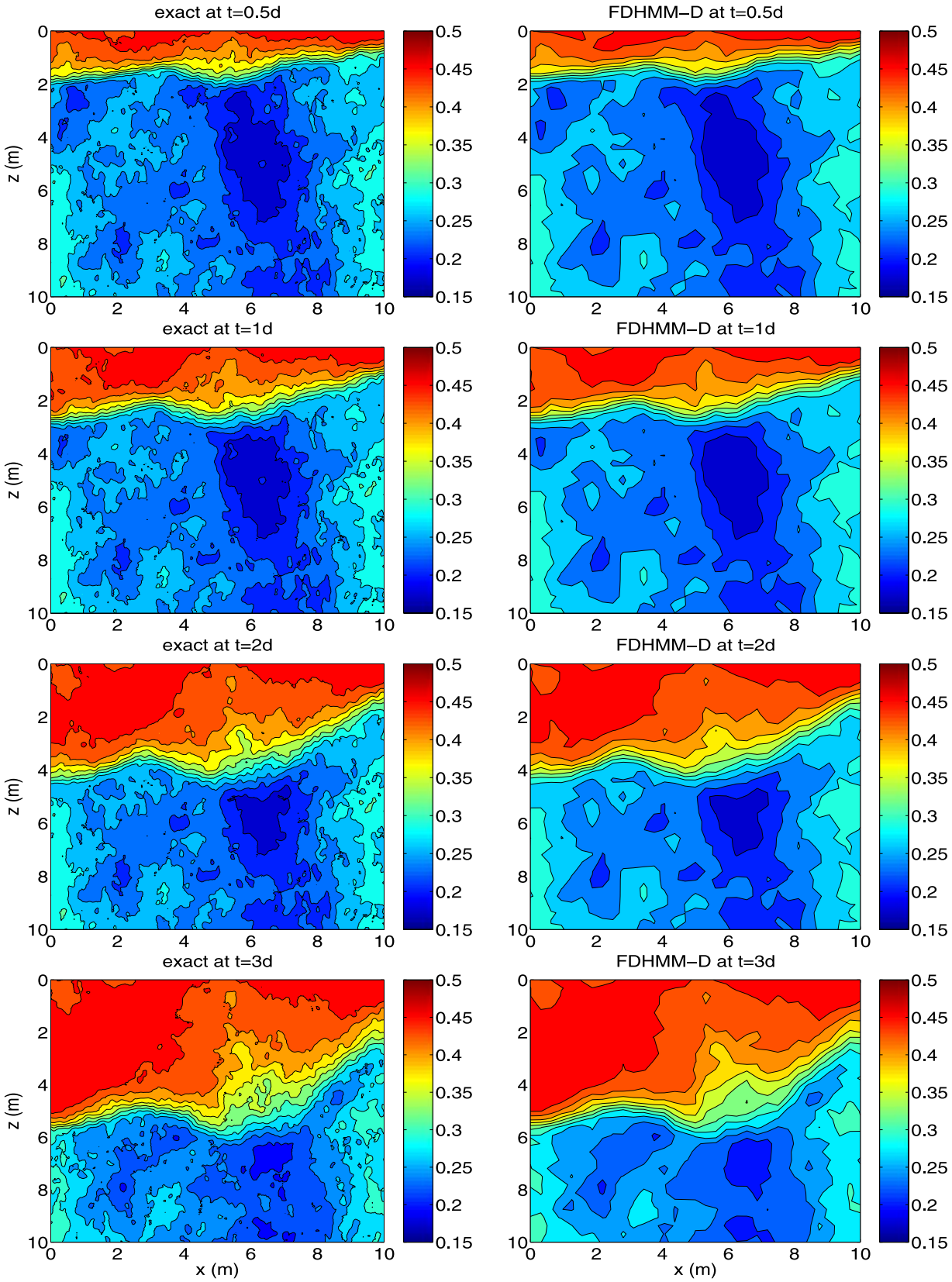

Figure 7. Comparison of water contents between the fine-scale model (left) and FDHMM-D (right) at times t = 0.5, 1, 2, 3 d (from top to bottom) for van Genuchten-Mualem model with Dirichlet infiltration boundary.

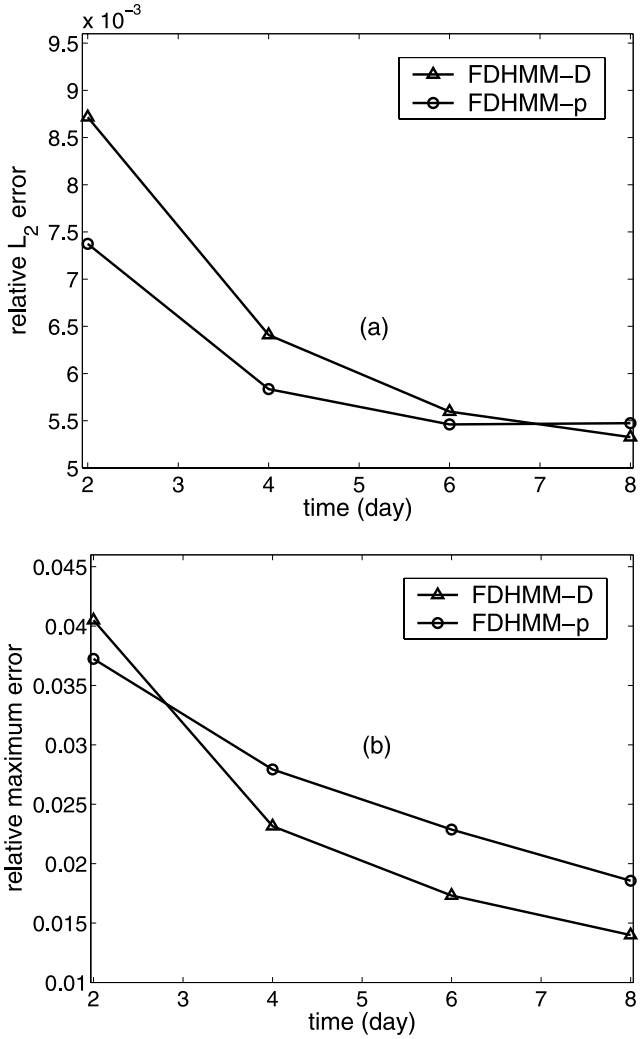

Figure 8. Relative (a) L_2 and (b) maximum errors between "exact" and two coarse solutions for van Genuchten-Mualem model with Neumann infiltration boundary.

3.1. Verification of Code

[40] The algorithm of section 2 has been implemented in a FORTRAN code. We verify this code by using the linearization model for unsaturated equation (1)

$$C\frac{\partial\psi}{\partial t} - \nabla\cdot[K_r\mathbf{K}_s(\mathbf{x})\nabla\psi] + \frac{K(\mathbf{x},\psi_1) - K(\mathbf{x},\psi_0)}{\psi_1 - \psi_0}\frac{\partial\psi}{\partial z} = 0, \quad (29)$$

with C, K_r, ψ_0 and ψ_1 constant, and $K(\mathbf{x},\psi_0)$, $K(\mathbf{x},\psi_1)$ calculated by using (2) and $K_s(\mathbf{x})$. We impose the following initial condition and boundary conditions for the test example:

$$\psi(x,z,0) = -10.0m, \text{ in } \Omega. \quad (30)$$

$$\begin{aligned}
&\text{Top} \quad \psi(x,0,t) = -1.0m, \quad 0 \le x \le 10m, t \ge 0,\\
&\text{Bottom} \quad \psi(x,10m,t) = -10.0m, \quad 0 \le x \le 10m, t \ge 0,\\
&\text{Left} \quad \tfrac{\partial\psi}{\partial x}|_{x=0} = 0, \quad 0 < z < 10m, t \ge 0,\\
&\text{Right} \quad \tfrac{\partial\psi}{\partial x}|_{x=10m} = 0, \quad 0 < z < 10m, t \ge 0.
\end{aligned} \quad (31)$$

Here the upper and lower boundaries of the solution domain are the Dirichlet boundaries, the other two boundary conditions are for no-flow boundaries.

[41] Let $C = 0.2\ \text{m}^{-1}$, $K_r = 0.2$, $\psi_0 = -10.0$ m, $\psi_1 = -1.0$ m, $n' = 1.6$ and $\alpha_v = 0.3\ \text{m}^{-1}$. Fix a time step size $\Delta t = 5.0 \times 10^{-4}$ d. If $K_s(\mathbf{x})$ has the following periodic form

$$K_s(x,z) = \frac{0.44}{2 + 1.8\sin(2\pi(2x - z)/1.25)}, \quad (32)$$

The relative errors of pressure head for FDHMM-D and FDHMM-p at times t = 0.5, 1, 2 and 3 d are showed in Figure 2. We observe that both FDHMM-D and FDHMM-p have about the same accuracy. If $K_s(\mathbf{x})$ has a random form, we assume that the geometric mean of K_s is 0.44 md^{-1}, the standard deviation of lnK_s is 1.2, and the correlation lengths λ_x and λ_z are 5.0 m and 3.0 m respectively. The relative errors of pressure head for FDHMM-D and FDHMM-p at times t = 0.5, 1, 2, and 3 d are showed in Figure 3. The errors of results of FDHMM-p are very close to those of FDHMM-D, both FDHMM-D and FDHMM-p give a reasonable accuracy.

[42] The correctness of the compiled code is verified by the above two linear examples. Next we use this verified code to simulate the transient unsaturated water flow problems with random coefficients for the nonlinear parabolic equation of Richards' type.

3.2. van Genuchten-Mualem Model With Dirichlet Infiltration Boundary

[43] Statistical parameters used to describe heterogeneous fields are loosely based on hydraulic parameters of silt according to USDA textural class [*Soil Survey Staff Division*, 1993]. Let $\bar{K}_s$, $\bar{\alpha}_v$ be the geometric means of K_s and α_v respectively, we take θ_s = 0.489 $\text{m}^3\ \text{m}^{-3}$, θ_r = 0.05 $\text{m}^3\ \text{m}^{-3}$, n' = 1.6 and $\bar{K}_s$ = 0.44 md^{-1}, $\bar{\alpha}_v$ = 0.3 m^{-1}. For the realization considered here the correlation lengths λ_x and λ_z are 5.0 m and 3.0 m, the standard deviations of lnK_s and $ln\alpha_v$ are 1.2 and 0.3, respectively. A realization of the random saturated conductivity field is plotted in Figure 4. This hydraulic conductivity K_s varies by over two orders of magnitude over the solution domain, from a minimum of 3.1×10^{-2} md^{-1} to a maximum of 23.1 md^{-1}. Figure 5 shows a realization of the model parameter α_v and the ratio of maximum to minimum for it is 5.2.

[44] Assume the test example has the same initial condition and boundary conditions used in section 3.1. Fix a time step size $\Delta t = 5.0 \times 10^{-4}$ d, and choose the van Genuchten-Mualem model as the constitutive relationship. The relative errors of pressure head for FDHMM-D and FDHMM-p at times t = 0.5, 1, 2, and 3 d are shown in Figure 6. Figure 6 indicates that both FDHMM-D and FDHMM-p give a reasonable accuracy in relative L_2 and maximum norms. FDHMM-D has a relative L_2 error of less than 1.7% and makes the relative maximum error monotonously decrease from 18.6% to 6.4%. Water content distributions in the whole soil profile at times t = 0.5, 1, 2, and 3 d obtained from the fine-scale model and FDHMM-D are plotted in Figure 7. We observe that FDHMM-D can capture the local microstructure at coarse mesh points.

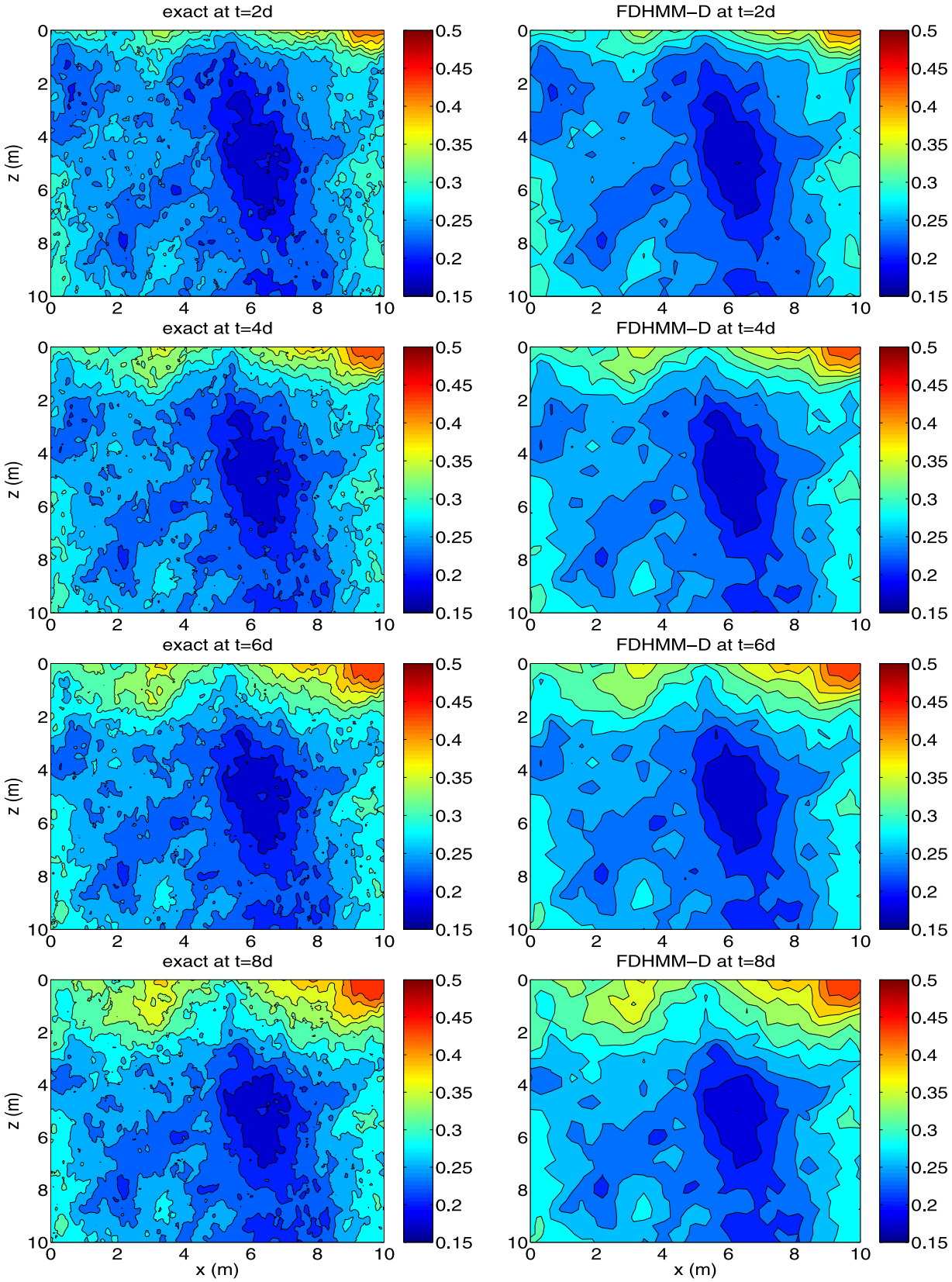

Figure 9. Comparison of water contents between the fine-scale model (left) and FDHMM-D (right) at times t = 2, 4, 6, 8 d (from top to bottom) for van Genuchten-Mualem model with Neumann infiltration boundary.

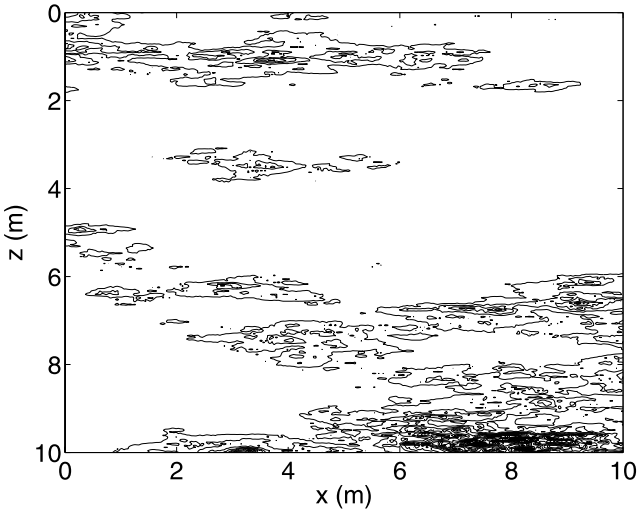

Figure 10. A realization of the random lognormal saturated conductivity field. The ratio of maximum to minimum is 4.0×10^3.

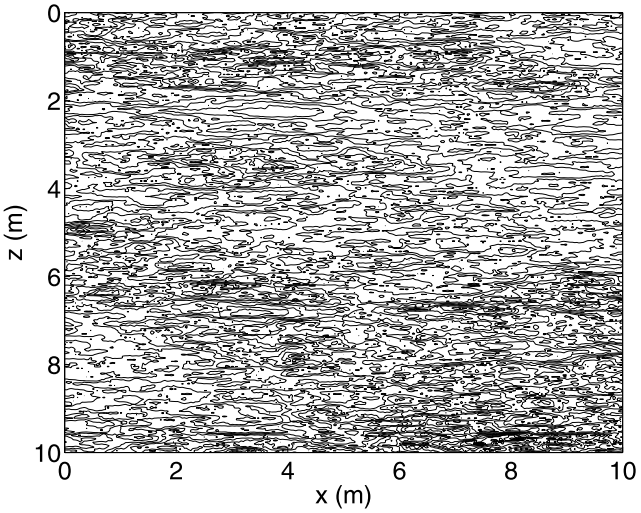

Figure 11. A realization of the random lognormal alpha field. The ratio of maximum to minimum is 8.0.

3.3. van Genuchten-Mualem Model With Neumann Infiltration Boundary

[45] We use the same test example discussed in section 3.2 except for top and bottom boundary conditions. In this section, boundary conditions are defined as follows

$$\begin{aligned}
&\text{Top} && -K(x,z,t)\tfrac{\partial(\psi-z)}{\partial z}|_{z=0} = q, \quad 0 \le x \le 10m, \quad t \ge 0,\\
&\text{Bottom} && \tfrac{\partial \psi}{\partial z}|_{z=10m} = 0, \quad 0 \le x \le 10m,\ t \ge 0,\\
&\text{Left} && \tfrac{\partial \psi}{\partial x}|_{x=0} = 0, \quad 0 < z < 10m,\ t \ge 0,\\
&\text{Right} && \tfrac{\partial \psi}{\partial x}|_{x=10m} = 0, \quad 0 < z < 10m,\ t \ge 0.
\end{aligned} \tag{33}$$

q is the constant infiltration rate and is slight as less than the minimum value of the saturated conductivity, here $q = 3.1 \times 10^{-2}$ md^{-1}. The lower boundary is for free drainage and the lateral boundaries are for no-flow conditions.

[46] Fix a time step size $\Delta t = 2.0 \times 10^{-3}$ d. Choose the van Genuchten-Mualem model as the constitutive relationship. Figure 8 plots the relative errors for FDHMM-D and FDHMM-p at times $t = 2$, 4, 6, and 8 d. As in the example discussed in section 3.2, both FDHMM-D and FDHMM-p give a satisfying accuracy. Moreover, the results obtained in this case are more accurate than those obtained in section 3.2. This is likely because the Neumann infiltration boundary condition is a softer boundary condition than the Dirichlet one, for the transient unsaturated water flow problem in silt, FDHMM is more powerful for the Neumann infiltration boundary than the Dirichlet infiltration boundary. We also note that FDHMM-D gives comparable accuracy with FDHMM-p. Water content distributions in the whole soil profile at times $t = 2$, 4, 6, and 8 d obtained from the fine-scale model and FDHMM-D are depicted in Figure 9. For FDHMM-D, it gives excellent agreement between the coarse mesh and fine mesh calculations.

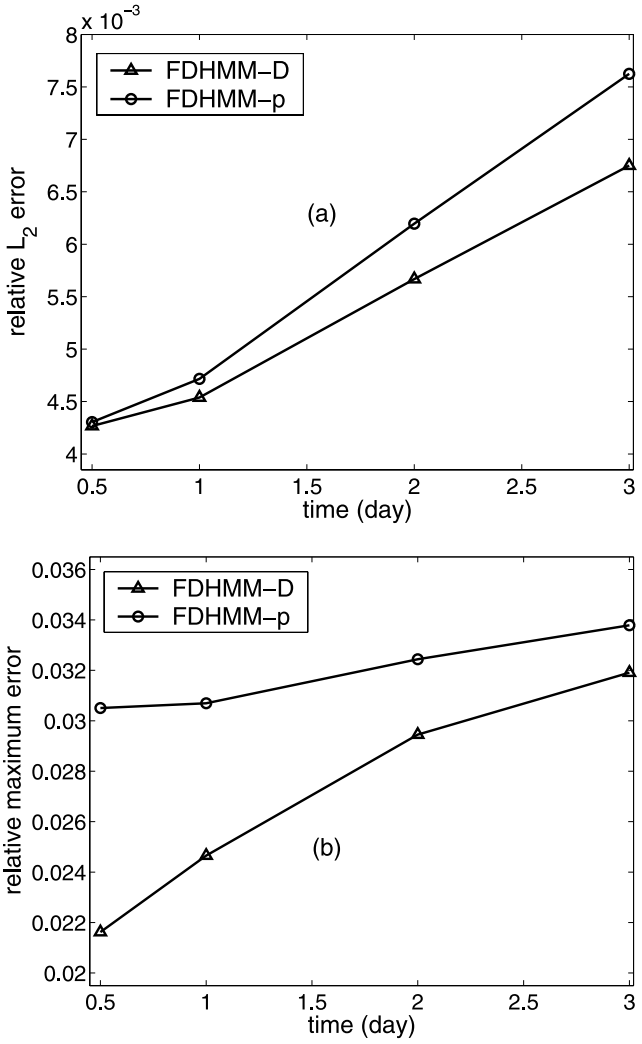

Figure 12. Relative (a) L_2 and (b) maximum errors between "exact" and two coarse solutions for Gardner-Basha model with Dirichlet infiltration boundary.

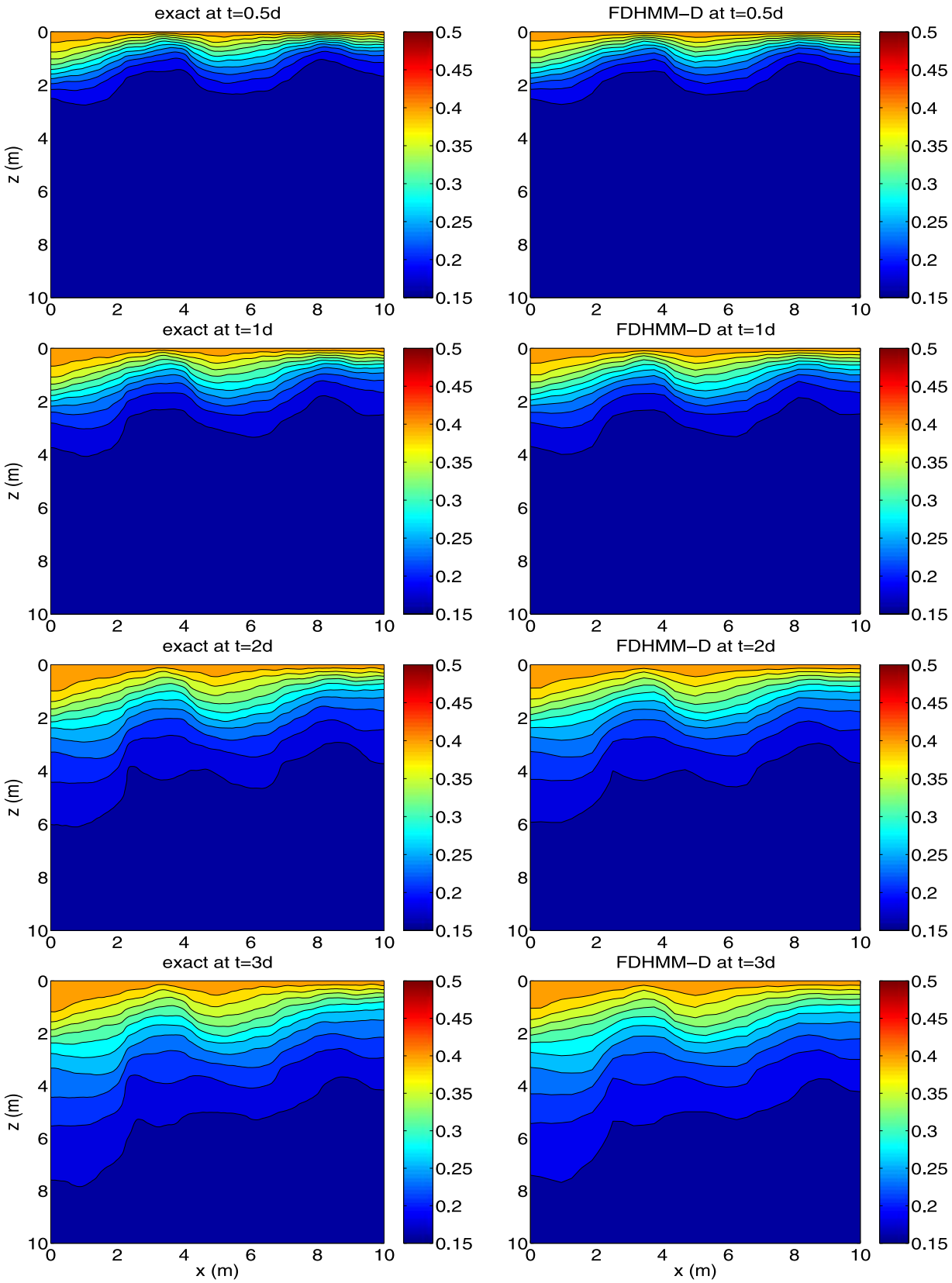

Figure 13. Comparison of water contents between the fine-scale model (left) and FDHMM-D (right) at times $t = 0.5$, 1, 2, 3 d (from top to bottom) for Gardner-Basha model with Dirichlet infiltration boundary.

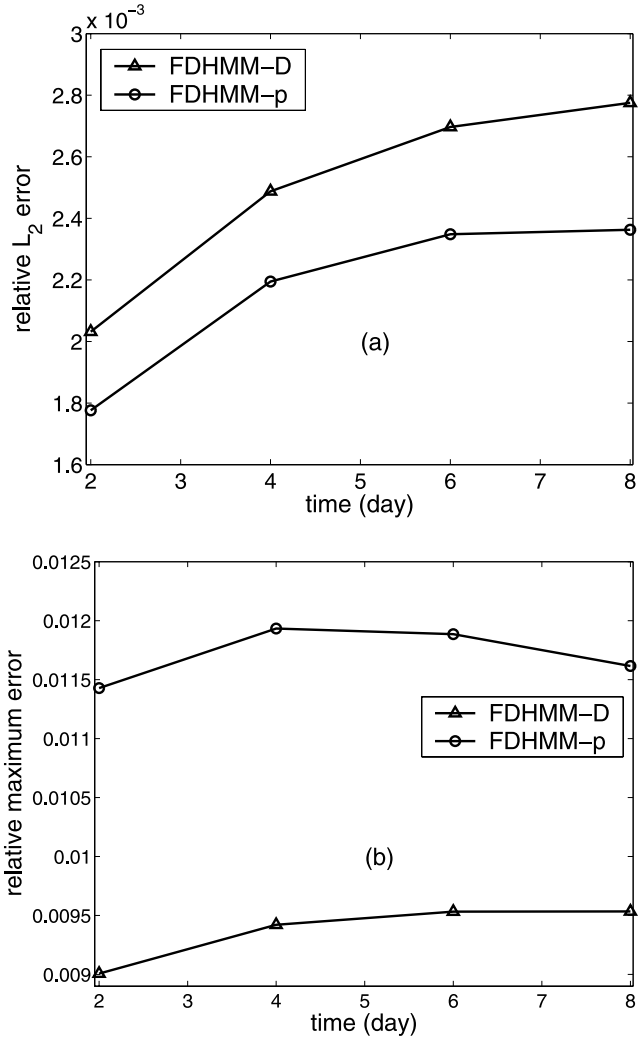

Figure 14. Relative (a) L_2 and (b) maximum errors between "exact" and two coarse solutions for Gardner-Basha model with Neumann infiltration boundary.

3.4. Gardner-Basha Model With Dirichlet Infiltration Boundary

[47] In this section, the statistical parameters used to describe heterogeneous fields are loosely based on hydraulic parameters of peat given by *Varado et al.* [2006]. Let $\bar{\alpha}_G$ be the geometric means of α_G, we take $\theta_s = 0.47\ m^3\ m^{-3}$, $\theta_r = 0.0\ m^3\ m^{-3}$, $\beta = 0.104\ m^{-1}$ and $\bar{K}_s = 0.053\ md^{-1}$, $\bar{\alpha}_G = 0.104\ m^{-1}$. For the realization considered here the correlation lengths λ_x and λ_z are 5.0 m and 1.0 m, the standard deviations of lnK_s and $ln\alpha_G$ are 1.2 and 0.3, respectively. The saturated hydraulic conductivity K_s varies by over three orders of magnitude over the solution domain and the ratio of maximum to minimum for α_G is 8.0. The random fields of K_s and α_G are respectively plotted in Figure 10 and Figure 11.

[48] We assume the test example based on the Gardner-Basha model with the same initial condition and boundary conditions used in section 3.1. Fix a time step size $\Delta t = 1.0 \times 10^{-3}$ d. Figure 12 plots the relative errors of pressure head for FDHMM-D and FDHMM-p at times $t = 0.5$, 1, 2, and 3 d. We note that the results indicated in Figure 12 are similar to those in Figure 6 and Figure 8, both FDHMM-D and FDHMM-p give a satisfying accuracy in relative L_2 and maximum norms. Moreover, FDHMM gives more accuracy in this test example than in the test example described in section 3.2. FDHMM-D gives the relative L_2 and maximum errors of less than 0.7% and 3.2% respectively. FDHMM-p gives the relative L_2 and maximum errors of less than 0.8% and 3.4% respectively. The reason may be that near the wetting front, gradient of slope of the Gardner water retention curve gives less change than that of the van Genuchten water retention curve, then near the wetting front the solutions by using the Gardner-Basha model are less change than those by using the van Genuchten-Mualem model. The results of FDHMM-D are slightly better accurate than those of FDHMM-p. Figure 13 shows the comparison of water content distributions in the whole soil profile at times $t = 0.5$, 1, 2, and 3 d between the fine-scale model and FDHMM-D. It illustrates excellent agreement between the water contents obtained by FDHMM-D and the water contents obtained by the fine-scale model.

3.5. Gardner-Basha Model With Neumann Infiltration Boundary

[49] In this section, we suppose that our test example has the same hydraulic parameters and random fields described in section 3.4 and has the same initial condition and boundary conditions used in section 3.3 except for the constant infiltration rate q. Here $q = 6.0 \times 10^{-4}\ md^{-1}$.

[50] Fix a time step size $\Delta t = 2.0 \times 10^{-3}$ d. Choose the Gardner-Basha model as the constitutive relationship. We show in Figure 14 the relative errors of solutions of FDHMM-D and FDHMM-p at times $t = 2$, 4, 6, and 8 d. Both FDHMM-D and FDHMM-p give a satisfying accuracy. FDHMM-D has relative L_2 and maximum errors of less than 0.3% and 1.0% respectively, FDHMM-p has relative L_2 and maximum errors of less than 0.3% and 1.2% respectively, the accuracies of both methods are comparable. We plot in Figure 15 water content distributions in the whole soil profile at times $t = 2$, 4, 6, and 8 d obtained from the fine-scale model and FDHMM-D. The water contents obtained by FDHMM-D give excellent agreement with the water contents obtained by the fine-scale model over the whole simulating time. Different from the previous examples, water contents near the infiltration front keep a decreasing trend because the constant infiltration rate q is too low.

4. Discussion

[51] While the discussed algorithm has a successful application on the test examples in section 3, we hope to know more about FDHMM in this section. We first consider the computational cost of FDHMM. Next dependence of algorithm error on cell size is discussed. Following this the global mass conservative property and the convergence behavior of FDHMM are illustrated. We also reconstruct the fine scale information from the coarse scale solution if it is necessary. For simplicity, our discussions are mainly based on the test example described in section 3.2, i.e., the case for the transient unsaturated water flow problem in the spatially random silty soil with the van Genuchten-Mualem model and the Dirichlet infiltration boundary.

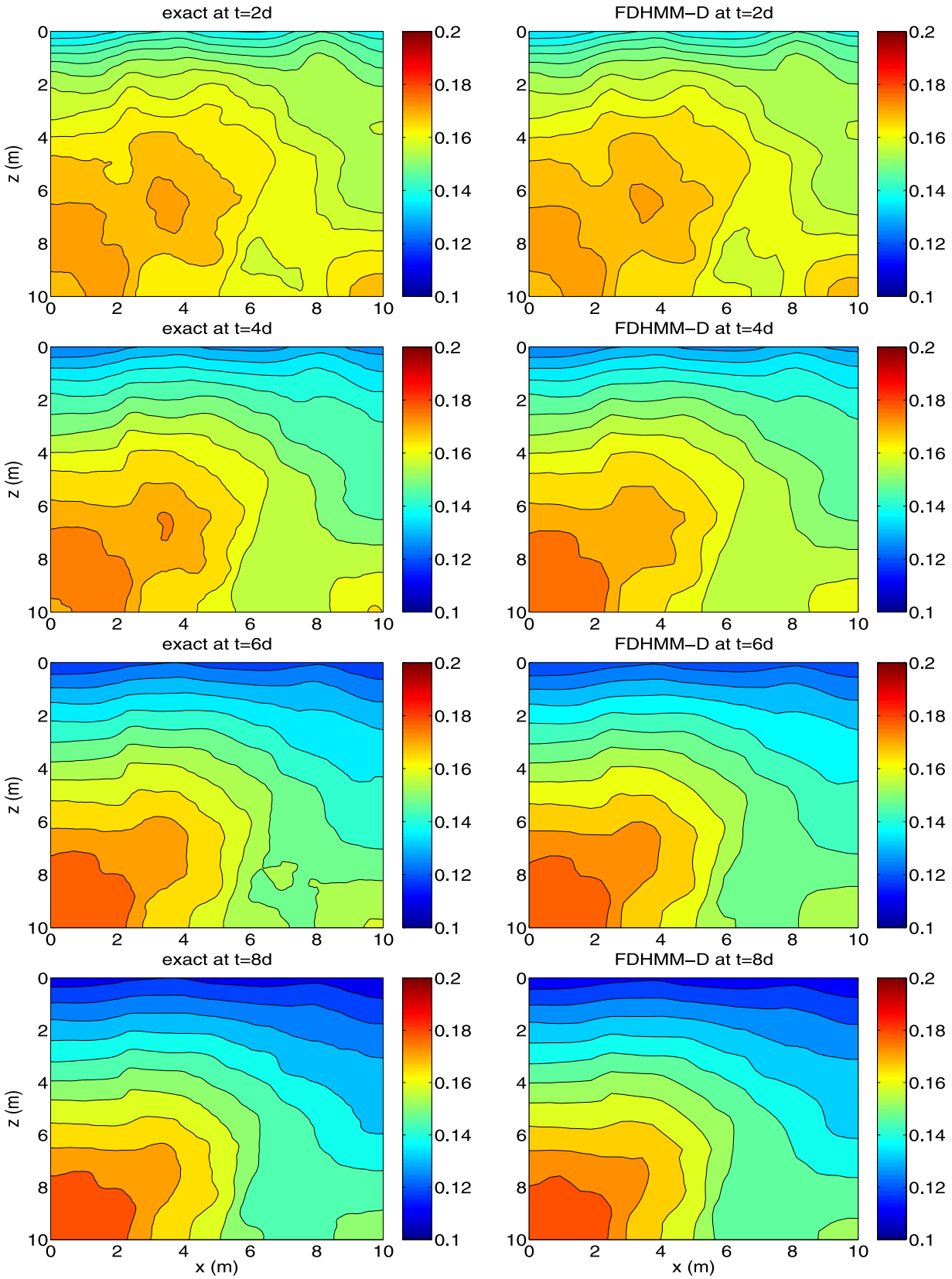

Figure 15. Comparison of water contents between the fine-scale model (left) and FDHMM-D (right) at times $t = 2, 4, 6, 8$ d (from top to bottom) for Gardner-Basha model with Neumann infiltration boundary.

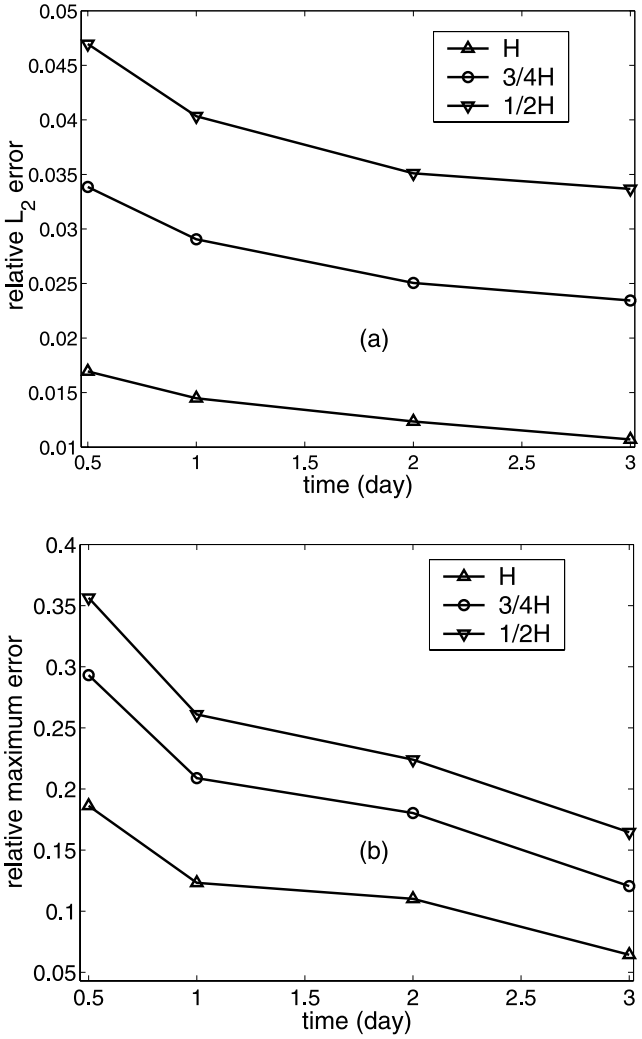

Figure 16. Relative (a) L_2 and (b) maximum errors between the fine-scale model and FDHMM-D for different cell sizes.

4.1. Computational Cost

[52] It is of interest to consider the computational requirements for the fine- and coarse-scale simulations. The first saving in memory storage in the FDHMM strategy is achieved by reducing the computation of the fine grid on the whole domain. The fine-scale global flow solution is decomposed into a series of cell problems, the main memory cost of FDHMM is the cost of solving of $2N(N-1)$ cell problems, when $\delta = H$, it has $(M-1)^2$ unknowns for FDHMM-D and has $(M+1)^2$ unknowns for FDHMM-p in every cell, the computation of these cell problems can be carried out sequentially, it can obtain an obvious decrease in memory. In addition, when $\delta = \frac{1}{2}H$, the coarse scheme needs to solve a series of small nonlinear algebra equation systems, while the fine scheme needs to solve a very large nonlinear algebra equation system. The computational time of solving a nonlinear algebra equation system may be nonlinear with its degrees of freedom, this may be a reason why FDHMM can save the computational time. For the specific problem, when $\delta = \frac{1}{2}H$, the results have been obtained on an IBM ThinkCentre running Windows XP Pro with Intel(R) Pentium(R)4 CPU 2.80 GHz processor, and 1 GB of RAM. Costs of memory using conventional finite difference method, FDHMM-D and FDHMM-p are about 35.0, 7.4, and 7.4 megabytes respectively, costs of CPU time using three above methods are about 3.3 h, 0.8 h and 3.2 h respectively. Compared with the computational cost of conventional finite difference method, in our test example, FDHMM-D can save about 78.9% memory and about 75.8% CPU time, FDHMM-p can save about 78.9% memory and about 3.0% CPU time. Moreover, this advantage will be embodied more obviously when the researched domain increases or number of fine mesh increases. Notice that each δ-cell computation in FDHMM is independent, so that the computation of the cell problems can be done in parallel. Since the macro computation is very fast the parallel implementation can highly speed up the computational time.

4.2. Dependence of Algorithm Error on Cell Size and Correlation Length

[53] As pointed out by *E et al.* [2003], the key to efficiency of such an approach is the possibility that the microscopic model does not have to be solved over the whole computational domain, but rather over a small region near where data estimation is carried out. Here, we will discuss the effects of different cell sizes on the results of FDHMM-D. For the transient unsaturated water flow problem described in section 3.2, we fix the coarse mesh size $H = 10/32$ m, and change cell size δ. Let $\delta = H$, $\frac{3}{4}H$, $\frac{1}{2}H$ respectively, the calculated results obtained by using different cell sizes at times $t = 0.5$, 1, 2, and 3 d are depicted in Figure 16. This figure indicates that a reasonable accuracy in eer_2 and eer_∞ norms is given by using three different cell sizes. The larger cell size is, the more accurate the results are. The results obtained under $\delta = H$ are the best, the results obtained under $\delta = \frac{3}{4}H$ are less accurate than those obtained under $\delta = H$, the results obtained $\delta = \frac{1}{2}H$ are the worst, but in this case FDHMM-D also has relative L_2 and maximum errors of less than 4.7% and 35.6% respectively. Figure 17 plots water content distributions in the whole soil profile at time $t = 2$ d obtained from the fine-scale model and FDHMM-D for different cell sizes. We observe that, for different cell sizes, FDHMM-D can capture the local microstructure at coarse mesh points. For the cases of $\delta = \frac{3}{4}H$ and $\delta = \frac{1}{2}H$, we actually use 87.5% and 50.0% of total data at the small scale respectively. This flexibility of choosing cell size means that FDHMM can be applied to more complicated problem for which the microstructure can be partly found beforehand.

[54] Also investigated is the influence of the spatial correlation length of random coefficients (K_s and α) on the accuracy of FDHMM. In the test example discussed in section 3.2, we consider three random fields with $\lambda_x = 5.0$ m and $\lambda_z = 3.0$ m, $\lambda_x = 20.0$ m and $\lambda_z = 10.0$ m, $\lambda_x = 100.0$ m and $\lambda_z = 20.0$ m respectively. The results of FDHMM-D for different random fields at times $t = 0.5$, 1, 2, and 3 d are plotted in Figure 18. Figure 18 indicates that, if cell size $\delta = H$ determined, the spatial correlation length of random coefficients under the given standard deviations $\sigma_{lnK} = 1.2$ and $\sigma_{ln\alpha_v} = 0.3$ has relatively little influence on the accuracy of FDHMM.

[55] From the above test examples, choosing $\delta = H$ may be preferred in unsaturated flow problems. Thus we may

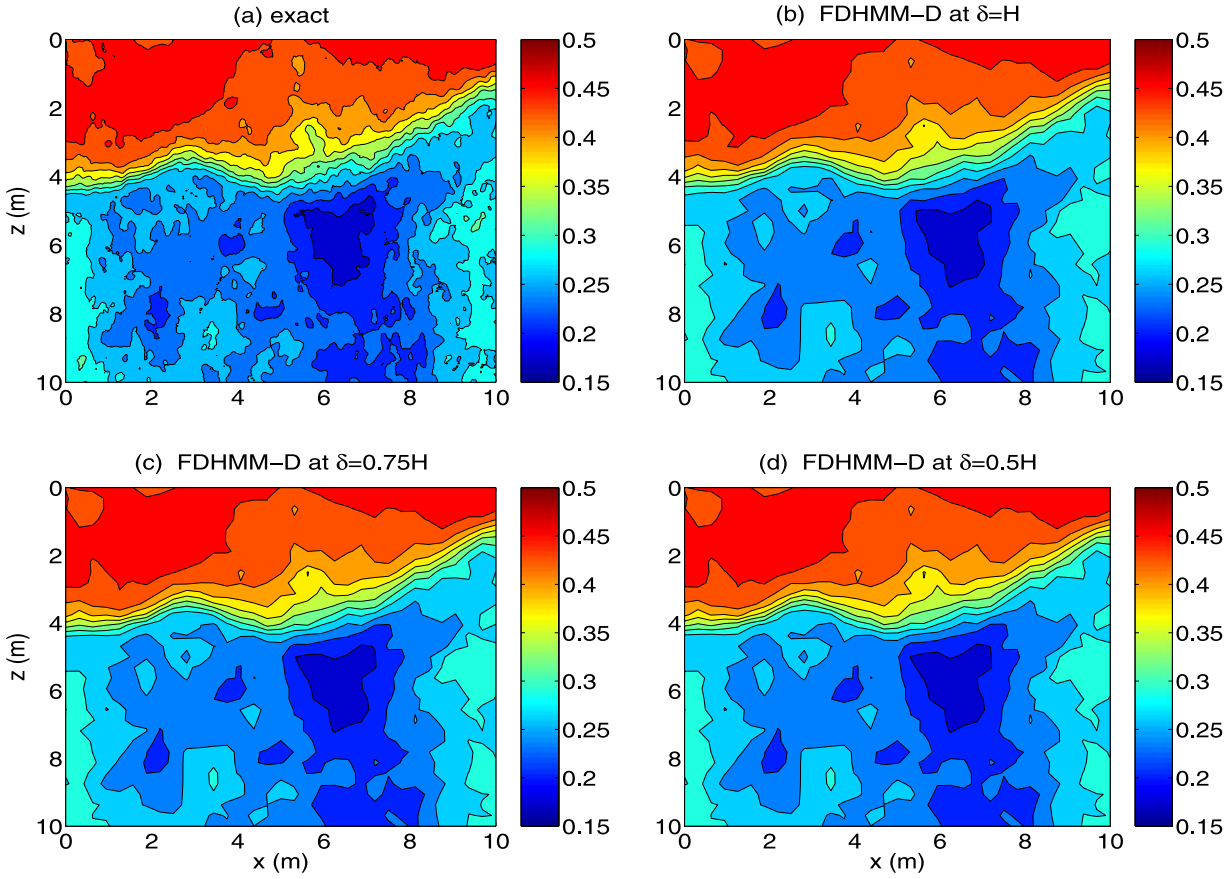

Figure 17. Water contents for (a) the fine-scale model and FDHMM-D in (b) $\delta = H$, (c) $\delta = \frac{3}{4}H$ and (d) $\delta = \frac{1}{2}H$ at time $t = 2d$.

choose cell size δ be equal to H if the microstructure has been completely found, we also may choose cell size δ such that $\delta = \frac{3}{4}H$, $\delta = \frac{1}{2}H$ or other suitable sizes if the microstructure cannot be completely found beforehand. In addition, cell size δ in the above all examples is actually smaller than the correlation length of random coefficients, it is different from the principle of choosing cell size in the linear problem presented by *Abdulle and E* [2003] and *E et al.* [2005]. It seems that there is a significant difference in the principle of choosing cell size between the unsaturated water flow problem and the saturated water flow problem.

4.3. Global Mass Conservative Property

[56] In FDHMM, we determine the macroscopic equation by estimating the macroscopic flux F using the integral of the fluxes at the fine mesh, in other words, we choose methodologically the finite volume approach as the macroscopic scheme. Thus FDHMM may satisfy the mass conservation law from the viewpoint of the flux balance. One measure of a numerical method is its ability to conserve global mass over the domain of interest. To measure the ability of the proposed method to conserve mass, let mass balance measure be defined as follows [*Celia et al.*, 1990]:

$$MB(t) = \frac{\text{total additional mass in the domain}}{\text{total net flux into the domain}}, \tag{34}$$

where the additional mass is measured with respect to the initial mass in the system. For our test example, this is calculated by

$$\begin{aligned} MB\left(t^{n+1}\right) = a\sum_{i=1}^{N+1}\sum_{j=1}^{N+1}\left(\Theta_{i,j}^{n+1} - \Theta_{i,j}^{0}\right) \Big/ \Bigg\{ \Delta t \sum_{l=1}^{n+1} \\ \cdot \Bigg\{ \sum_{j=1}^{N} \left(K_{N+\frac{1}{2},j}^{l} \frac{\Psi_{N+1,j}^{l} - \Psi_{N,j}^{l}}{a} - K_{1+\frac{1}{2},j}^{l} \frac{\Psi_{2,j}^{l} - \Psi_{1,j}^{l}}{a} \right) \\ + \sum_{i=1}^{N} \Bigg[K_{i,N+\frac{1}{2}}^{l} \left(\frac{\Psi_{i,N+1}^{l} - \Psi_{i,N}^{l}}{a} - 1 \right) \\ - K_{i,1+\frac{1}{2}}^{l} \left(\frac{\Psi_{i,2}^{l} - \Psi_{i,1}^{l}}{a} - 1 \right) \Bigg] \Bigg\} \Bigg\}, \end{aligned} \tag{35}$$

where $\Theta_{i,j}^{0}$ is the initial macroscopic volumetric water content at coarse mesh point (i,j).

[57] The influence of maintaining mass balance is plotted in Figure 19. The solution of FDHMM-D exhibits mass balance errors of less than 3.7% although it costs 6000 time steps to attain the end of the simulating time $t = 3$ d. This fact indicates that FDHMM satisfies the global mass conservative property under the Dirichlet infiltration boundary.

4.4. Convergence Behavior

[58] Convergence should be a necessary condition for FDHMM as a good numerical method. Fix $\delta = H$, the

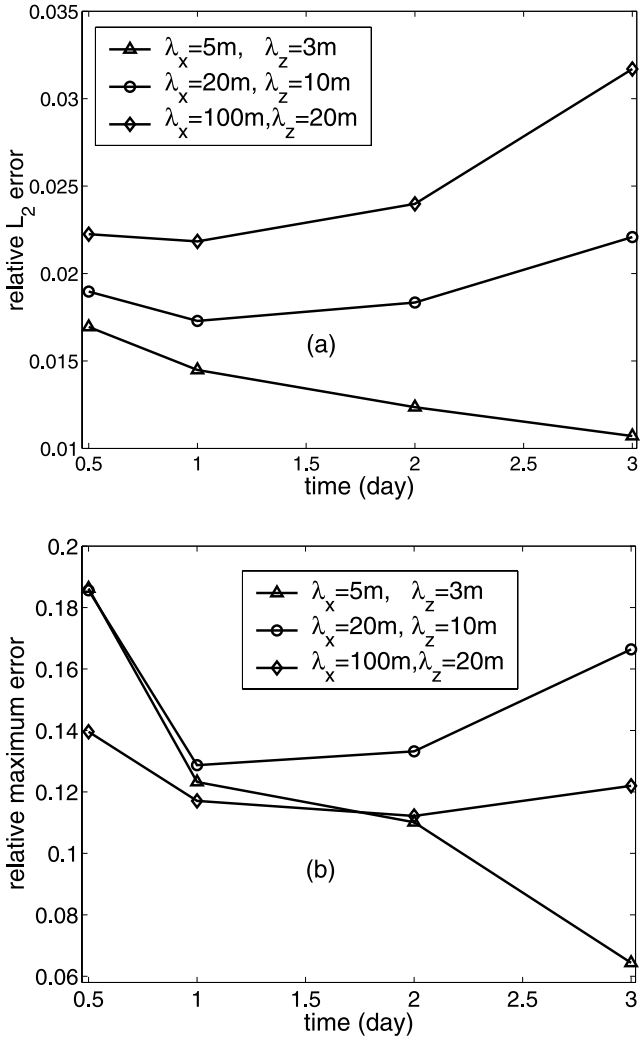

Figure 18. Relative (a) L_2 and (b) maximum errors between the fine-scale model and FDHMM-D for different correlation lengths.

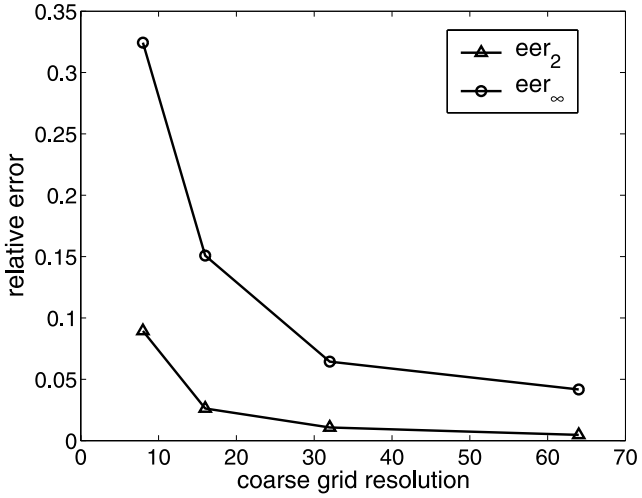

Figure 20. Relative L_2 and maximum errors of the solution of FDHMM-D at t = 3 d for coarse grids with 8 × 8, 16 × 16, 32 × 32 and 64 × 64 elements.

relative errors for coarse meshes with 8 × 8, 16 × 16, 32 × 32 and 64 × 64 elements at t = 3 d are plotted in Figure 20, here the coarse solutions are obtained by FDHMM-D. Notice that both eer_2 and eer_∞ monotonically decrease as the total number of coarse elements increases and tend to zero. It implies that the solution of FDHMM converges as the coarse mesh is refined.

4.5. Reconstruction of the Fine Scale Information

[59] The heterogeneity determines asymmetry of information what we need to grasp. It can sometimes be important to recover information about the fine scale at some points outside the coarse mesh. We reconstruct the fine mesh solution by bilinear interpolating in the fine mesh, i.e., the fine mesh solution is obtained by simple linear reconstruction based on the coarse mesh solution. If the coarse solution $\Psi^n_{i,j}$ is known, r denotes the ratio of the size of coarse grid cell to that of fine grid cell,

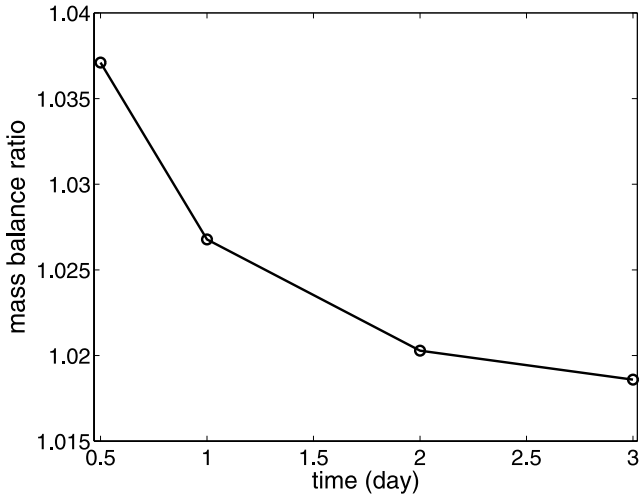

Figure 19. Mass balance results for van Genuchten-Mualem model with Dirichlet infiltration boundary in silt.

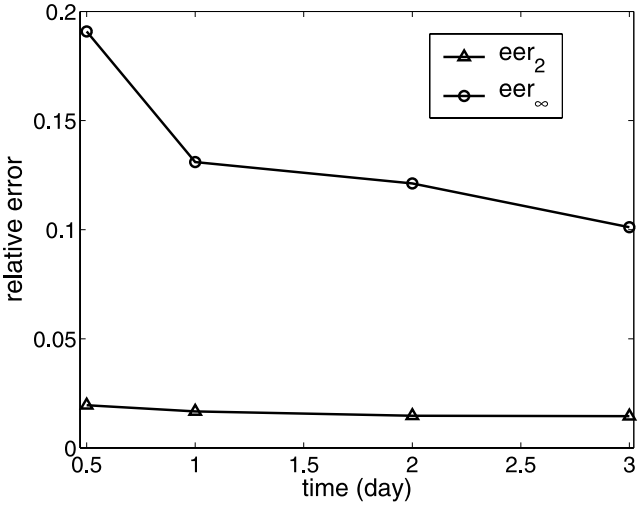

Figure 21. Relative errors between "exact" and reconstructed fine-scale solutions for van Genuchten-Mualem model with Dirichlet infiltration boundary.

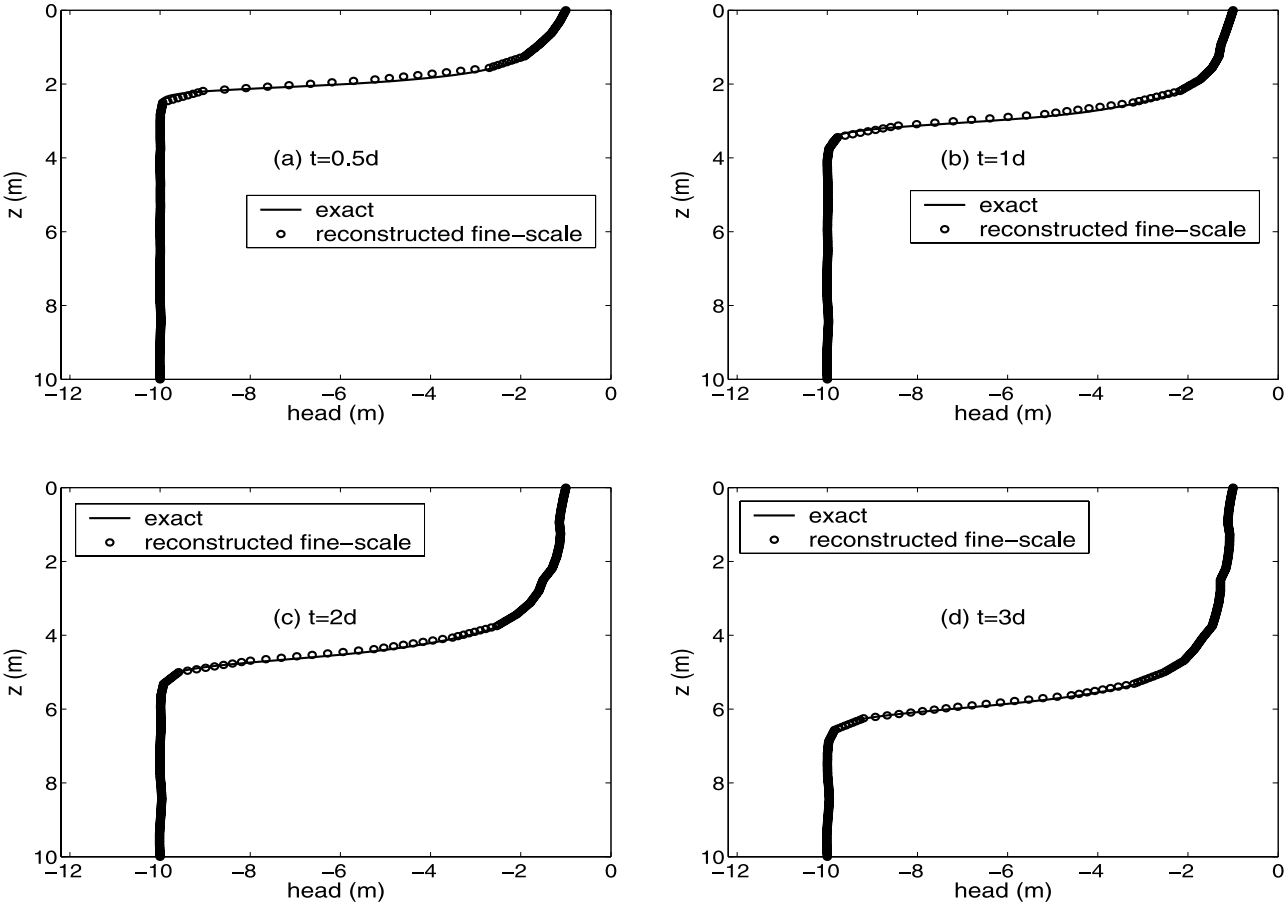

Figure 22. "Exact" and reconstructed fine-scale solutions at times (a) $t = 0.5$ d, (b) $t = 1$ d, (c) $t = 2$ d and (d) $t = 3$ d in section $x = 5$ m for van Genuchten-Mualem model with Dirichlet infiltration boundary.

for any reconstructed fine-scale solution $\psi^n_{k',l'}$, the bilinear interpolating function is

$$\psi^n_{k',l'} = \Psi^n_{i,j} + \frac{k'_0}{r}\left(\Psi^n_{i+1,j} - \Psi^n_{i,j}\right) + \frac{l'_0}{r}\left(\Psi^n_{i,j+1} - \Psi^n_{i,j}\right) + \frac{k'_0 l'_0}{r^2}\left(\Psi^n_{i+1,j+1} + \Psi^n_{i,j} - \Psi^n_{i+1,j} - \Psi^n_{i,j+1}\right), \tag{36}$$

where

$$k' = (i-1)r + k'_0 + 1, \quad k'_0 = 0, 1, \cdots, r-1, \qquad l' = (j-1)r + l'_0 + 1, \quad l'_0 = 0, 1, \cdots, r-1, \tag{37}$$

in which $i-1$ and $j-1$ are the integer parts of k'/r and l'/r, respectively.

[60] We did the reconstruction starting with the solution of FDHMM-D on a coarse 32×32 mesh. Figure 21 shows the calculated results of reconstructed fine scale solution for the transient unsaturated water flow problem described in section 3.2 at times $t = 0.5$, 1, 2, and 3 d. This figure indicates that the reconstructed fine scale solution gives a satisfying accuracy in eer_2 and eer_∞ norms. The comparison between the "exact" solution and the reconstructed fine scale solution at times $t = 0.5$, 1, 2, and 3 d in section $x = 5$ m is illustrated in Figure 22. The similar result of Figure 21 is found, FDHMM illustrates a high accuracy in reconstruction of the fine scale information.

4.6. Application Scope and Limitations for FDHMM

[61] Our test examples above are mainly based on hydraulic parameters of silt and peat, the numerical experiments also show that FDHMM has been successful for the transient unsaturated water flow problem in loam and loamy sand if we emphasize the relative L_2 error and ignore the relative maximum error, but the proposed method fails to deal with the transient unsaturated water flow problem in sand. Several test examples based on the van Genuchten-Mualem model with the Dirichlet infiltration boundary are done to hold out this result. The study domain and its discretization are the same as those of section 3.

[62] For loam, we loosely take hydraulic parameters of loam according to USDA textural class: $\theta_s = 0.399$ m^3 m^{-3}, $\theta_r = 0.061$ m^3 m^{-3}, $n' = 1.5$, $\bar{K}_s = 0.12$ md^{-1}, $\sigma_{lnKs} = 1.0$, $\bar{\alpha}_v = 0.9$ m^{-1}, $\sigma_{ln\alpha_v} = 0.3$, $\lambda_x = 4.0$ m, $\lambda_z = 1.0$ m. Let the initial pressure head be $\psi(x,z,0) = -10.0$ m; the upper boundary is $\psi(x,0,t) = -0.5$ m, the bottom boundary is $\psi(x,10\text{ m},t) = -10.0$ m, the other boundary conditions are for no-flow boundaries. Fix a time step size $\Delta t = 2.0 \times 10^{-3}$d. Over the study time $T = 12$ d, FDHMM-D can control the relative L_2 error less than 9.9%, but FDHMM-D cannot control the relative maximum error which is about 70.0%. Figure 23 plots water content distributions in the whole soil

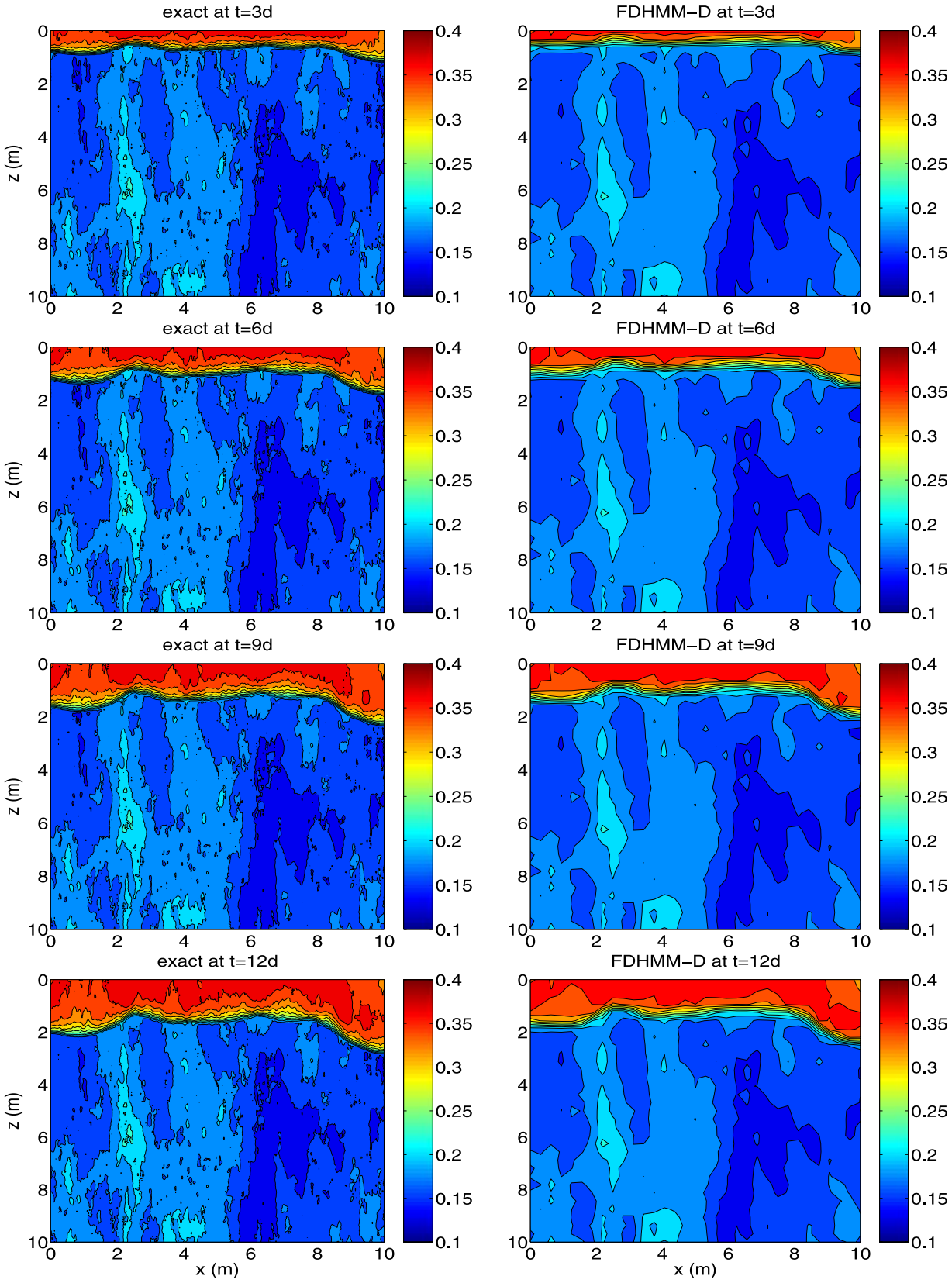

Figure 23. Comparison of water contents between the fine-scale model (left) and FDHMM-D (right) at times $t = 3, 6, 9, 12$ d (from top to bottom) for the unsaturated flow problem with van Genuchten-Mualem model and Dirichlet infiltration boundary in loam.

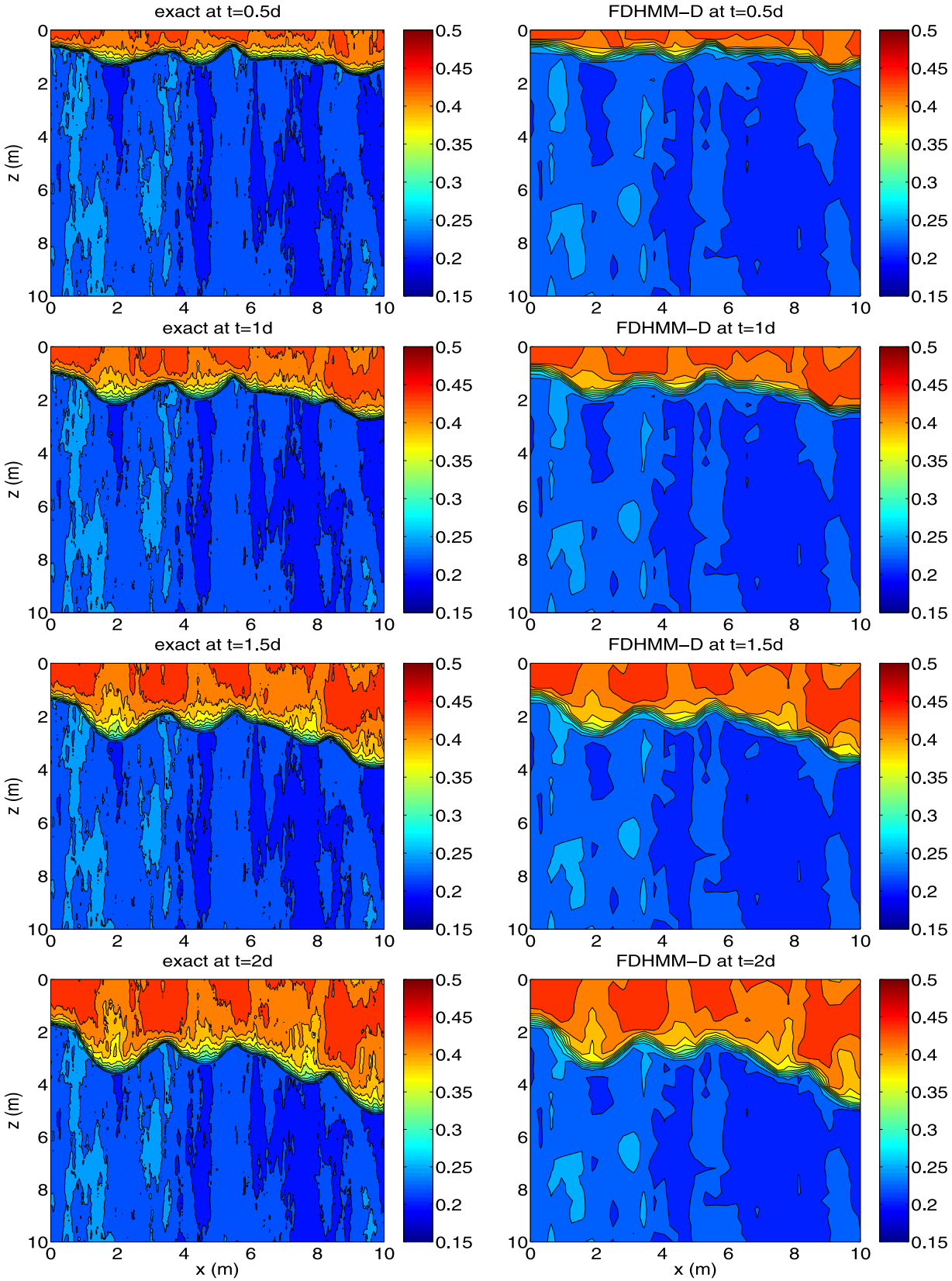

Figure 24. Comparison of water contents between the fine-scale model (left) and FDHMM-D (right) at times t = 0.5, 1, 1.5, 2 d (from top to bottom) for the unsaturated flow problem with van Genuchten-Mualem model and Dirichlet infiltration boundary in loamy sand.

profile at times t = 3, 6, 9, and 12 d obtained from the fine-scale model and FDHMM-D. It illustrates that the water contents obtained by FDHMM-D are in rough agreement with those obtained by the fine-scale model.

[63] For loamy sand, we loosely consider the data reported by *Diersch* [2002]: θ_s = 0.47 m^3 m^{-3}, θ_r = 0.17 m^3 m^{-3}, n' = 2.0, $\bar{K}_s$ = 0.75 md^{-1}, σ_{lnKs} = 1.0, $\bar{\alpha}_v$ = 1.0 m^{-1}, $\sigma_{ln\alpha_v}$ = 0.2, λ_x = 4.0 m, λ_z = 0.5 m. Let the initial pressure head be $\psi(x,z,0) = -5.0$ m; the upper and lower boundaries of the solution domain are the Dirichlet boundaries, head on the top side is −0.5 m and on the bottom side is −5.0 m, the other boundary conditions are for no-flow boundaries. Use a constant time step of $\Delta t = 5.0 \times 10^{-4}$ d. Over the study time T = 2 d, FDHMM-D can control eer_2 less than 6.7%, FDHMM-D also fails to handle eer_∞ which waves from 48.5% to 64.5%. Two test examples above mean that FDHMM-D can simulate a general tendency of the transient unsaturated water flows in loam and loamy sand for the specific examples. Figure 24 shows water content distributions in the whole soil profile at times t = 0.5, 1, 1.5, and 2 d obtained from the fine-scale model and FDHMM-D. We find that the water contents obtained by FDHMM-D can approximate those obtained by the fine-scale model.

[64] For sand, we loosely take hydraulic parameters of sand according to USDA textural class: θ_s = 0.375 m^3 m^{-3}, θ_r = 0.053 m^3 m^{-3}, n' = 3.2, $\bar{K}_s$ = 6.43 md^{-1} σ_{lnKs} = 1.0, $\bar{\alpha}_v$ = 3.52 m^{-1}, $\sigma_{ln\alpha_v}$ = 0.2, λ_x = 1.0 m, λ_z = 0.3 m. Let the initial pressure head be $\psi(x,z,0) = -5.0$ m; the upper and lower boundaries of the solution domain are the Dirichlet boundaries, head on the top side is −0.3 m and on the bottom side is −5.0 m; the other boundary conditions are for no-flow boundaries. For the study time T = 2 d, use a constant time step of $\Delta t = 5.0 \times 10^{-4}$ d. While t = 0.5 d, eer_2 and eer_∞ of the results of FDHMM-D attain to 30.7% and 95.0% respectively. Moreover, eer_2 of the results of FDHMM-D raises to 46.7% at t = 2 d. FDHMM-D fails to work in this test example.

5. Conclusion

[65] The finite difference heterogeneous multiscale method has been extended for solving transient unsaturated water flow problems in random porous media. The correctness of the compiled code is verified by using the linearization model of Richards' equation, the numerical experiments demonstrate that both FDHMM-D and FDHMM-p have about the same accuracy for the linear cases. A set of test examples, involving five soil textures, two constitutive relationships and two infiltration boundary conditions, are applied to test our scheme. For the transient unsaturated water flow problems in silt with the van Genuchten-Mualem model and the Dirichlet or Neumann infiltration boundary, our numerical experiments give convincing evidence that the FDHMM is effective to solve these problems accurately, the same conclusion is also arrived at applying FDHMM to simulate the transient unsaturated water flow problems in peat with the Gardner-Basha model and the Dirichlet or Neumann infiltration boundary. For the transient unsaturated water flow problem in silt with the van Genuchten-Mualem model, FDHMM is more powerful with the Neumann infiltration boundary than the Dirichlet infiltration boundary, the same result is found for the unsaturated water flow problems in peat with the Gardner-Basha model. In our numerical experiments, FDHMM-D often gives comparable accuracy with FDHMM-p. For the transient unsaturated water flow problems in loam and loamy sand with the van Genuchten-Mualem model and the Dirichlet infiltration boundary, FDHMM-D can also simulate a general tendency of the flows, however, FDHMM-D fails to work for the transient unsaturated water flow problem in sand with the van Genuchten-Mualem model and the Dirichlet infiltration boundary. For the transient unsaturated water flow problem in silt with the van Genuchten-Mualem model and the Dirichlet infiltration boundary, the spatial correlation length of random coefficients under the specific standard deviation tested may not play an important role in the accuracy of FDHMM, cell size δ may be chosen to be equal to H for the case in which the microstructure has been completely found beforehand, it also may be chosen to be equal to $\frac{3}{4}H$ or $\frac{1}{2}H$ for cases in which the microstructure can only be partly found beforehand. Based on an efficient coupling between the macroscopic and microscopic models, when $\delta = \frac{1}{2}H$, FDHMM can offer a big saving in the memory storage, and FDHMM-D can save the computational time, that is, FDHMM-D need only about one-fourth of the computational cost of standard finite difference method for the transient unsaturated water flow problem in silt with the van Genuchten-Mualem model and the Dirichlet infiltration boundary. In addition, our results indicate that, for the transient unsaturated water flow problem in silt with the van Genuchten-Mualem model and the Dirichlet infiltration boundary, FDHMM satisfies the global mass conservative property, and has the global convergence property, and also shows a high accuracy in reconstruction of the fine scale information.

[66] Our study is limited to 2-D unsaturated water flow through specific heterogeneous soils. In the future, we plan to further develop this algorithm for simulating unsaturated water flow problems in more soils with heterogeneity.

[67] **Acknowledgments.** Funding for this study was provided by the National Key Basic Research Special Funds (NKBRSF, 2006CB403406), China and by the National Natural Science Foundation of China grant 50779064. We thank the anonymous reviewers for their constructive comments.

References

Aarnes, J., V. Kippe, and K.-A. Lie (2005), Mixed multiscale finite elements and streamline methods for reservoir simulation of large geomodels, *Adv. Water Resour.*, *28*, 257–271.

Abdulle, A., and W. E (2003), Finite difference heterogeneous multiscale method for homogenization problems, *J. Comput. Phys.*, *191*, 18–39.

Allen, M. B., and C. Murphy (1985), A finite element collocation method for variably saturated flows in porous media, *Numer. Methods Partial Diff. Equations*, *3*, 229–239.

Babuška, I. (1976a), Solution of interface by homogenization, *I, II, SIAM, J. Numer. Anal.*, *7*, 603–645.

Babuška, I. (1976b), Homogenization and its applications, mathematical and computational problems, in *Numerical Solutions of Partial Differential Equations-III, (SYNSPADE 1975, Maryland, May 1975*), edited by B. Hubbard, pp. 89–116, Academic Press, New York.

Babuška, I. (1977), Solution of interface by homogenization, *III, SIAM J. Numer. Anal.*, *8*, 923–937.

Basha, H. A. (1999), Multidimensional linearized nonsteady infiltration with prescribed boundary conditions at the soil surface, *Water Resour. Res.*, *35*(1), 75–83.

Celia, M. A., E. T. Bouloutas, and R. L. Zarba (1990), A general mass-conservative numerical solution for the unsaturated flow equation, *Water Resour. Res.*, *26*(7), 1483–1496.

de Zeeuw, P. M. (1990), Matrix-dependent prolongations and restrictions in a blackbox multigrid solver, *J. Comput. Appl. Math.*, *33*, 1–27.

Diersch, H. J. G. (2002), *WASY Software FEFLOW 5.0 (Finite Element Subsurface Flow and Transport Simulation System)-Reference Manual*, WASY Institute for Water Resour. Plann. and Syst. Res. Ltd, Berlin.

Durlofsky, L. J. (1991), Numerical calculation of equivalent grid block permeability tensors for heterogeneous porous media, *Water Resour. Res.*, *27*(5), 699–708.

Durlofsky, L. J., Y. Efendiev, and V. Ginting (2007), An adaptive local-global multiscale finite volume element method for two-phase flow simulations, *Adv. Water Resour.*, *30*, 576–588.

E, W., and B. Engquist (2003), The heterogeneous multiscale methods, *Comm. Math. Sci.*, *1*(1), 87–133.

E, W., B. Engquist, and Z. Huang (2003), Heterogeneous multiscale method: A general methodology for multiscale modeling, *Phy. Rev. B*, *67*, doi:10.1103/PhysRevB.67.092101.

E, W., P. B. Ming, and P. W. Zhang (2005), Analysis of the heterogeneous multiscale method for elliptic homogenization problems, *J. Am. Math. Soc.*, *18*(1), 121–156.

Efendiev, Y., and A. Pankov (2004), Numerical homogenization of nonlinear random parabolic operators, *SIAM Multiscale Model. Simul.*, *2*(2), 237–268.

Efendiev, Y., T. Y. Hou, and V. Ginting (2004), Multiscale finite element methods for nonlinear problems and their applications, *Commun. Math. Sci.*, *2*(4), 553–589.

Farthing, M. W., C. E. Kees, T. S. Coffey, C. T. Kelley, and C. T. Miller (2003), Efficient steady state solution techniques for variably saturated groundwater flow, *Adv. Water Resour.*, *26*, 833–849.

Freeze, R. A. (1975), A stochastic conceptual analysis of one-dimensional groundwater flow in nonuniform homogeneous media, *Water Resour. Res.*, *11*(5), 725–741.

Gardner, W. R. (1958), Some steady state solution of unsaturated moisture flow equations with applications to evaporation from a water table, *Soil Sci.*, *85*(4), 228–232.

Gelhar, L. W. (1986), Stochastic subsurface hydrology from theory to applications, *Water Resour. Res.*, *22*(9), 135–145.

Gutjahr, A. L., B. Bullard, S. Hatch, and L. Hughson (1994), Joint conditional simulations and the spectral approach for flow modeling, *Stoch. Hydrol. Hydr.*, *8*, 79–108.

Haverkamp, R., and M. Vauclin (1979), A note on estimating finite difference interblock hydraulic conductivity values for transient unsaturated flow problems, *Water Resour. Res.*, *15*, 181–187.

He, X., and L. Ren (2005), Finite volume multiscale finite element method for solving the groundwater flow problems in heterogeneous porous media, *Water Resour. Res.*, *41*, W10417, doi:10.1029/2004WR003934.

He, X., and L. Ren (2006a), A multiscale finite element linearization scheme for the unsaturated flow problems in heterogeneous porous media, *Water Resour. Res.*, *42*, W08417, doi:10.1029/2006WR004905.

He, X., and L. Ren (2006b), A modified multiscale finite element method for well-driven flow problems in heterogeneous porous media, *J. Hydrol.*, *329*, 674–684.

Hornung, U., and W. Messing (1983), Truncation errors in the numerical solution of horizontal diffusion in saturated/unsaturated media, *Adv. Water Resour.*, *6*, 165–168.

Hou, T. Y., and X. H. Wu (1997), A multiscale finite element method for elliptic problems in composite materials and porous media, *J. Comput. Phys.*, *134*, 169–189.

Hou, T. Y., X. H. Wu, and Z. Cai (1999), Convergence of a multiscale finite element method for elliptic problems with rapidly oscillating coefficients, *Math. Comput.*, *68*, 913–943.

Koltermann, C. E., and S. M. Gorelick (1996), Heterogeneity in sedimentary deposits: A review of structure-imitating, process-imitating, and descriptive approaches, *Water Resour. Res.*, *32*(9), 2617–2658.

Lewandowska, J., A. Szymkiewicz, K. Burzynski, and M. Vauclin (2004), Modeling of unsaturated water flow in double-porosity soils by the homogenization approach, *Adv. Water Resour.*, *27*, 283–296.

Mantoglou, A., and L. W. Gelhar (1987), Stochastic modeling of large-scale transient unsaturated flow systems, *Water Resour. Res.*, *23*(1), 37–46.

Mantoglou, A., and J. L. Wilson (1982), The turning bands method for simulation of random fields using line generation by a spectral method, *Water Resour. Res.*, *18*(5), 1379–1394.

Miller, C. T., C. Abhishek, and M. W. Farthing (2006), A spatially and temporally adaptive solution of Richards' equation, *Adv. Water Resour.*, *29*, 525–545.

Mualem, Y. (1976), A new model for predicting the hydraulic conductivity of unsaturated porous media, *Water Resour. Res.*, *12*(3), 513–522.

Neuman, S. P., and S. Orr (1993), Prediction of steady state flow in nonuniform geologic media by conditional moments: exact nonlocal formalism effective conductivities, and weak approximation, *Water Resour. Res.*, *29*(2), 341–346.

Rathfelder, K., and L. M. Abriola (1994), Mass conservative numerical solutions of the head-based Richards equation, *Water Resour. Res.*, *30*(9), 2579–2586.

Russo, D., and M. Bouton (1992), Statistical analysis of spatial variability in unsaturated parameters, *Water Resour. Res.*, *28*(7), 1911–1925.

Soil Survey Staff Division (1993), *Soil Survey Manual, USDA Handb.*, vol. 18. U. S. Gov. Print. Office, Washington, D. C.

Tompson, A. F. B., and L. W. Gelhar (1990), Numerical simulation of solute transport in three-dimensional, randomly heterogeneous porous media, *Water Resour. Res.*, *26*(10), 2541–2562.

Tompson, A. F. B., R. Ababou, and L. W. Gelhar (1989), Implementation of the three-dimensional turning bands random field generator, *Water Resour. Res.*, *25*, 2227–2243.

van Genuchten, M. T. (1980), A closed-form equation for predicting the hydraulic conductivity of unsaturated soils, *Soil Sci. Soc. Am. J.*, *44*, 892–898.

van Genuchten, M. T. (1982), A comparison of numerical solutions of the one-dimensional unsaturated-saturated flow and mass transport equations, *Adv. Water Resour.*, *5*, 47–55.

Varado, N., I. Braud, P. J. Ross, and R. Haverhamp (2006), Assessment of an efficient numerical solution of the 1D Richards' equation on bare soil, *J. Hydrol.*, *323*, 244–257.

Winston, R. B. (1999), MODFLOW-related freeware and shareware resources on the Internet, *Comput. Geosci.*, *25*, 377–382.

Ye, S., Y. Xue, and C. Xie (2004), Application of the multiscale finite element method to flow in heterogeneous porous media, *Water Resour. Res.*, *40*, W09202, doi:10.1029/2003WR002914.

Yeh, T. C., L. W. Gelhar, and A. L. Gutjahr (1985), Stochastic analysis of unsaturated flow in heterogeneous soils. Part I: Statistically isotropic media, *Water Resour. Res.*, *21*(4), 447–456.

Yue, X., and W. E (2005), Numerical methods for multiscale transport equations and application to two-phase porous media flow, *J. Comput. Phys.*, *210*, 656–675.

Yue, X., and W. E (2007), The local microscale problem in the multiscale modeling of strongly heterogeneous media: Effects of boundary conditions and cell size, *J. Comput. Phys.*, *222*, 556–572.

Zhang, R., J. Yang, and Z. Ye (1996), Solute transport through the vadose zone: A field study and stochastic analyses, *Soil Sci.*, *161*, 270–277.

F. Chen and L. Ren, Department of Soil and Water Sciences, China Agricultural University, No. 2 West Yuanmingyuan Road, Haidian District, Beijing 100094, China. (renl@mx.cei.gov.cn)